

Meta-modeling game for deriving theoretical-consistent, micro-structural-based traction-separation laws via deep reinforcement learning

Kun Wang WaiChing Sun *

October 26, 2018

Abstract

This paper presents a new meta-modeling framework to employ deep reinforcement learning (DRL) to generate mechanical constitutive models for interfaces. The constitutive models are conceptualized as information flow in directed graphs. The process of writing constitutive models are simplified as a sequence of forming graph edges with the goal of maximizing the model score (a function of accuracy, robustness and forward prediction quality). Thus meta-modeling can be formulated as a Markov decision process with well-defined states, actions, rules, objective functions and rewards. By using neural networks to estimate policies and state values, the computer agent is able to efficiently self-improve the constitutive model it generated through self-playing, in the same way AlphaGo Zero (the algorithm that outplayed the world champion in the game of Go) improves its gameplay. Our numerical examples show that this automated meta-modeling framework not only produces models which outperform existing cohesive models on benchmark traction-separation data, but is also capable of detecting hidden mechanisms among micro-structural features and incorporating them in constitutive models to improve the forward prediction accuracy, which are difficult tasks to do manually.

1 Introduction

Constitutive responses of interfaces are important for a wide spectrum of problems that involve spatial domain with embedded strong discontinuity, such as fracture surfaces [Rice, 1968, Park et al., 2009, Wang and Sun, 2017, Bryant and Sun, 2018], slip lines [Rabczuk and Areias, 2006, Borja and Foster, 2007], joints [Elices et al., 2002] and faults [Ohnaka and Yamashita, 1989, Wang and Sun, 2018, Sun and Wong, 2018]. While earlier modeling efforts, in particular those involving the modeling of cohesive zones, often solely focus on mode I kinematics, the mixed mode predictions of traction-separation law relations are critical for numerous applications, ranging from predicting damage upon impacts [Ortiz and Pandolfi, 1999], to predicting seismic events [Rudnicki, 1980]. Recent work by Park et al. [2009] provide a comprehensive account of the major characteristics of traction-separation laws and conclude that, while there are differences in details, most of the traction-separation laws obey a number of universal principles, such as the indifference of any superimposed rigid-body motion, the finite work required to create new surface, the existence of characteristics length scales, and the vanishing of cohesive traction with sufficient separations.

In the case where the loading history is not monotonic, constitutive responses of interfaces often become path-dependent. For instance, geomaterials, such as fault gauges, are known to exhibit rate- and state-dependent frictional responses [Paterson and Wong, 2005, Sun, 2013, Borja, 2013, Wang

*Corresponding author: WaiChing Sun, Assistant Professor, Department of Civil Engineering and Engineering Mechanics, Columbia University, 614 SW Mudd, Mail Code: 4709, New York, NY 10027 wsun@columbia.edu

et al., 2016, Na and Sun, 2017]. While there are phenomenological models designed to capture the path-dependent responses of the interfaces, a recent trend that gains increasing popularity is to replace the phenomenological traction-separation laws with computational homogenization procedure to capture the responses of materials with heterogeneous microstructures (cf. Moës et al. [2003], Hirschberger et al. [2008, 2009]). Nevertheless, as pointed out previously in Wang and Sun [2018], the major issue of applying hierarchical multiscale coupling on interfacial problems is the increasing computational demand due to the large number of required representative elementary simulations, a trade-off that is widely known in FEM² [Feyel, 2003] and other homogenization-based multiscale methods, such as FEM-DEM [Sun et al., 2011b,a, Fish, 2013, Sun et al., 2013a, Wang and Sun, 2015, Liu et al., 2016b, Kuhn et al., 2015, Wang and Sun, 2016, Wu et al., 2018].

To overcome this computational barrier, surrogate models are often derived to replicate the homogenized responses of sub-scale simulations [Kirane and Ghosh, 2008, Verhoosel et al., 2010, Keshavarz and Ghosh, 2013, Panchal et al., 2013, Faisal et al., 2014, Liu et al., 2016a, Tallman et al., 2017]. Nevertheless, since surrogate models are often constitutive laws hand-crafted by modelers to incorporate morphology-dependent features [Liu et al., 2016a], deriving, verifying and validating a surrogate model that can incorporate the essential information to yield macroscopic predictions with sufficient accuracy and robustness remain difficult and time-consuming. Data-driven models such as Le et al. [2015], Bessa et al. [2017], Versino et al. [2017], Kafka et al. [2018] and Wulfinghoff et al. [2018] attempted to overcome this issue via supervised machine learning (e.g. neural network [Lefik and Schrefler, 2002], symbolic regression model [Versino et al., 2017]) and unsupervised machine learning (e.g. dimensional reduction, feature extraction and clustering [Bessa et al., 2017, Wulfinghoff et al., 2018]).

In particular, recent work by Wang and Sun [2018] attempted to resolve this issue by building a generic recurrent neural network that can easily incorporate different types of sub-scale information (e.g. porosity, fabric tensor, and relative displacement) to predict traction. This technique uses the concept of directed graph on the transfer learning approach (cf. Pan et al. [2010]) in which multiple neural networks trained to make predictions on other physical quantities (e.g. relationship between porosity and fabric tensor) are re-used to generate additional inputs for predicting traction. However, the determination of the optimal input information (in addition to the displacement jump history) and configurations of information flow that enhances the prediction accuracy still requires a time-consuming trial-and-error task (cf. Section 4.3 Wang and Sun [2018]).

In this work, we introduce a general artificial intelligence approach to automate the creation and validation of traction-separation models. Unlike the previous approach in which neural networks are often used to either identify material parameters or create black-box constitutive laws, this work focuses on leveraging the capacity of a computer to improve via self-playing, a technique commonly referred as (deep) reinforcement learning in the computer science community [Sutton, 1992, Silver et al., 2016, 2017b]. In the past two years, the functionality of algorithms automatically generated from deep reinforcement learning have achieved remarkable success. In many cases, the demonstrated capacities were thought to be impossible in the past. For instance, the algorithm trained by deep reinforcement learning created by a company called DeepMind is able to outperform human experts in Go, Chess and Atari games. The most exciting part of this achievement is that, unlike previous AI such as the IBM Deep Blue, the deep reinforcement learning does not rely on hand-crafted policy evaluation functions and is therefore applicable to different kinds of games once they are defined and implemented.

This success motivates this research of proposing a meta-modeling approach where deep reinforcement learning may generate constitutive laws for (1) a given set of data, (2) a well-defined objective, and (3) a given set of universal principles. To achieve this goal, we recast the process of writing a constitutive model as a game with components suitable for deep reinforcement learning, involving a sequence of actions completely compatible with the stated rules (i.e., the law of physics). First, we define the model score, which could be any objective function suitable for a given task. For instance, this objective can be minimizing the discrepancy between calibrated experimental results and *blind predictions* measured by a norm, or a constrained optimization problem that gives considerations on

other attributes such as consistency, speed, and robustness [Wang et al., 2016]. Once the score (i.e., the objective) is clearly defined, we then implement the rules, which are the universal principles of mechanics, such as material frame indifference, laws of thermodynamics. These rules are applied in an environment in which scores are sampled. In the case of traction-separation law, the environment is simply the validation process itself.

Following this, we then define the action space which consists of a number of actions available for the modelers to write constitutive models. Once the action space and the model score are defined, we leverage the directed graph modeling technique to generate a state. The state at the end of each game represents a constitutive model automatically generated from the computer algorithm. In reality, the action space could be of very high dimensions such that manually deriving, implementing, verifying and validating all possible configurations are not feasible. This situation is similar of playing the games of chess and Go where the number of possible combinations of decisions or moves (each can be represented by a decision tree) remains finite but is so enormous that it is not possible to seek the optimal moves by exhausting all possibilities [Shannon, 1950].

With the state, action, rule and objective defined, the most critical part is to assign reward for each action. In principle, if the action space is of very low dimension, i.e., there are not many ways to model the physical processes, then the reward for each action can be determined by exhausting all the possible model configurations. However, in the case of writing a complex traction-separation model, we cannot evaluate the quality of the model until its predictions are compared with benchmark data. Therefore, the ability to approximate the reward for each action (in our case the modeling choices) without the need to evaluate all the available options becomes crucial for the success of the meta-modeling approach.

The deep reinforcement learning is therefore ideal for us to achieve this goal. We can approximate the rewards via neural networks and the Bellman expectation equation [Bellman, 1957, Dolcetta and Ishii, 1984]. By repeatedly generating new constitutive laws (i.e., playing the game of writing models), the agent will use the reward obtained from each played game, in analogy with the binary game result (win/loss) at the end of a Go game, to update the action probabilities and value functions to improve the agent’s ability to write good constitutive laws. Through sufficient self-plays, the reinforcement learning algorithm then improves the modeling choices it made over time until it is ready for predictions.

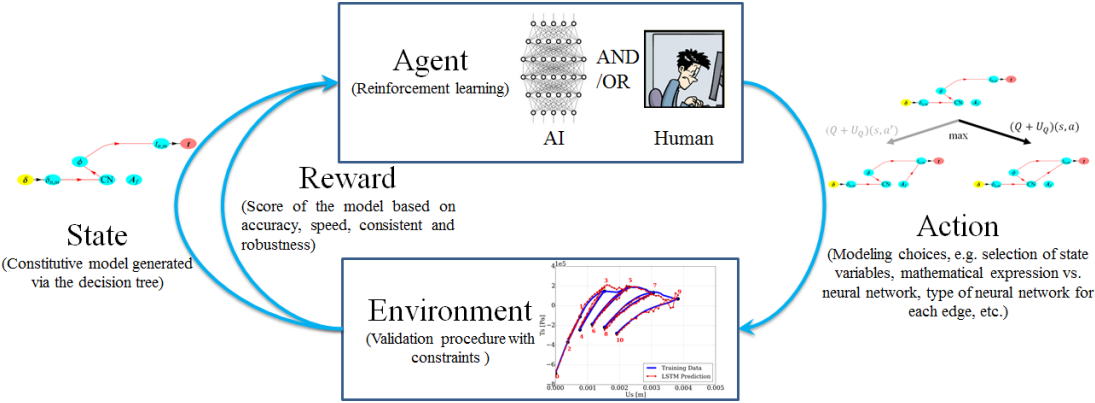


Figure 1: Scheme of the reinforcement learning algorithm in which an agent interacts with environment and receives rewards. Through exploration, the agent then determines better actions to achieve a particular goal defined by the reward. In our case, the reward is the score which represents the quality of the forward prediction, the action is any possible activities required to derive a constitutive law, and the environment is the procedure that compares the predictions with the benchmark data.

There are a few major upshots for this approach. First, once the reinforcement learning algorithm is established, it can serve as a model generator without any human intervention. Second, since

we regard the validation process as the environment component of the reinforcement learning, the performance of a resultant model is simultaneously evaluated and therefore validations are always a part of the model writing process. Third, the meta-modeling approach may easily embed any existing model generated by domain experts into the action space without re-implementing a new model. These unique capabilities enable us to have an unbiased tool to evaluate how well existing models fulfill a particular objective. Furthermore, since the model generation procedure is automated once an objective function is defined, this work may potentially eliminate the need of writing multiple incremental models for the same materials over time. Finally, this modeling approach is particularly powerful for discovering hidden physical coupling mechanisms that are otherwise too subtle to detect with human observation.

The rest of the paper is organized as follows. We first review the directed graph approach that enables us to generate and utilize a decision tree to represent the modeling process (Section 2). The definition of model scores is then described in Section 3. We then provide a formal definition of a game invented to generate traction-separation laws for predictions (Section 4). This is followed by a description on how to use the reinforcement learning for the traction-separation law generation (Section 5). Two numerical experiments are then used to showcase the performance of the automated meta-modeling approach using synthetic data from microscale discrete element simulations (Section 6). The major findings are then summarized in the conclusions.

2 Representing traction-separation law in directed graph

In this section, we introduce a building block for a simplified and extensible game that generates traction-separation laws by considering the relationships among different types of data collected from sub-scale simulations. In this game, the goal is to find a specific way to link different types of data such that a score function is maximized. Before we introduce the formal definition of the game, one necessary step is to recast the algorithm that leads to predictions from constitutive laws as a network of unidirectional information flow, i.e., a directed graph (also referred as digraph) [Sun et al., 2013b, 2014, Sun, 2015, Salinger et al., 2016, Wang and Sun, 2018]. Recall that a digraph $D = (V, E)$ is an ordered pair of non-empty finite sets which consists of a vertex set V and an edge set E [Bang-Jensen and Gutin, 2008]. Each edge connects a source vertex (tail) to a target vertex (head). Following the treatment in Sun [2015] and Wang and Sun [2018], the following **rules** are applied to generate the traction-separation law.

1. The traction t is placed as the only leaf of the digraph (i.e., the vertex that is not source to any other vertices).
2. The displacement jump δ is placed as the only root of the digraph (i.e., the vertex that is not target of any other vertices).
3. There may exist isolated vertices in the digraph, i.e., some internal variables or microstructural features between δ and t may not contribute to the final completed digraph and the corresponding constitutive model.
4. The digraph is acyclic, which means that there must be no cycle in the digraph.
5. If a vertex has sources or targets connected to it, it must be on at least one of the paths leading from δ to t . This ensures that an internal variable, once considered, is fully incorporated into the final constitutive model.

In the previous published work (cf. Sun [2015], Wang and Sun [2018]), we prescribed theoretical models or, in some cases, neural network models to create linkages and enforce the hierarchy among physical quantities (e.g. porosity-permeability relation). While this treatment is convenient for software engineering and code design [Salinger et al., 2016], this approach only works if we have

a prior knowledge about the relationships among the physical quantities. While one may presumably make ad hoc assumptions to complete the models, such a treatment is often at the expense of robustness. Another possible remedy is to gather all the measurement and data one may possibly obtain from observations and experiments, then find the key mechanisms that incorporate the most essential physics (e.g. the critical state plasticity for soil). This latter approach can be re-expressed as a problem in the directed graph in which we only know the elements of the vertex set but have no idea whether and how these vertices are connected, except that the traction is the leaf and the displacement jump is the root of the directed graph. Note that, in reality, the creation of a deterministic constitutive law does not only limit at determining connections among vertices (physical quantities), but also includes finding hidden vertices and appropriate edges. These actions are not modeled in this paper, but will be considered in future studies. Furthermore, while our focus in this paper is on deriving the traction-separation laws, in principle, the idea can be easily extended to other problems, such as the stress-strain relation for bulk materials, the porosity-temperature-fabric-tensor-permeability relations for porous media, among others.

For demonstration purposes, we consider a constitutive law $\mathbf{t}(\delta, \mathbf{q})$ that predicts the traction vector \mathbf{t} based on the history of the displacement jump δ over a cohesive or cohesive-frictional surface with the normal direction vector being \mathbf{n} . \mathbf{q} is a collection of state variables with n degrees of freedom, i.e., $q_1, q_2, q_3, \dots, q_n$. We use sub-scale discrete element simulations to generate synthetic data and attempt to create a traction-separation model which can replicate the constitutive responses of complex loading histories.

Imposing restrictions of material frame indifference and assuming isotropic cohesive-frictional surface, the traction-separation model can be simplified to [Ortiz and Pandolfi, 1999]

$$\mathbf{t}(\delta, \mathbf{q}) = \mathbf{t}(\delta_n, \delta_m, \mathbf{q}), \quad (1)$$

where $\delta_n = \delta \cdot \mathbf{n}$ and $\delta_m = |\delta_m| = |\delta - \delta_n \mathbf{n}|$. Hence, the traction \mathbf{t} is related to its components t_n and t_m that

$$\mathbf{t}(\delta, \mathbf{q}) = t_n(\delta_n, \delta_m, \mathbf{q})\mathbf{n} + t_m(\delta_n, \delta_m, \mathbf{q})\frac{\delta_m}{\delta_m}. \quad (2)$$

The internal variables in \mathbf{q} , if the cohesive surface is composed of a thin layer of granular materials, can be chosen among a large set of geometrical measures on micro-structural attributes [Sun et al., 2013a, Kuhn et al., 2015]. In this work, we first manually select the following measures to be the intermediate vertices (the vertices that are neither the leaves nor the roots) to make forward predictions on the traction vector.

- Porosity ϕ , the ratio between the volume of the void and the total volume of a representative volume element (RVE) of the material layer.
- Coordination number $CN = N_{\text{contact}}/N_{\text{particle}}$ where N_{contact} is the number of particle contacts and N_{particle} is the number of particles in the RVE.
- Fabric tensor $\mathbf{A}_f = \frac{1}{N_{\text{contact}}} \sum_{c=1}^{N_{\text{contact}}} \mathbf{n}^c \otimes \mathbf{n}^c$, where \mathbf{n}^c is the normal vector of a particle contact c , $c = 1, 2, \dots, N_{\text{contact}}$ in the RVE.
- Strong fabric tensor $\mathbf{A}_{sf} = \frac{1}{N_{\text{strongcontact}}} \sum_{c=1}^{N_{\text{strongcontact}}} \mathbf{n}^c \otimes \mathbf{n}^c$, where \mathbf{n}^c is the normal vector of a strong particle contact (having a compressive normal force greater than mean contact force) c , $c = 1, 2, \dots, N_{\text{strongcontact}}$ in the RVE.

All particle contacts inside the RVE can form a graph with particles as vertices and interactions as edges. Some quantitative measures of this graph of connectivity can be included in the internal variables \mathbf{q} as additional microstructural characteristics. Here, we focus on four measures, which are computed using the software package NetworkX (Hagberg et al. [2008]), and their detailed explanations can be found in the software documentation.

- d_a , degree assortativity, a scalar value between -1 and 1 measuring the similarity of connections in the graph with respect to the node degree.
- c_t , transitivity coefficient, $c_t = 3 \frac{n_{\text{triangles}}}{n_{\text{triads}}}$, the fraction between the number of triangles and the number of triads present in contact graph.
- l_{sp} , average shortest path length in the contact graph.
- ρ_g , density of the graph, $\rho_g = \frac{2m}{n(n-1)}$, where n is the total number of nodes and m is the total number of edges in the graph.

To sum up, in the digraph representations of traction-separation models, δ is the root and t is the leaf, and currently we consider q to be a subset of the following set of physical quantities $\{\delta_{n,m}, t_{n,m}, \phi, CN, A_f, A_{sf}, d_a, c_t, l_{sp}, \rho_g\}$. For the edges, we classify them as either "definitions" (such as $t_{n,m} \rightarrow t$, $\delta \rightarrow \delta_{n,m}$) which are determined by universal principles in mechanics and should not be modified, or the "phenomenological relations" (such as $\delta_{n,m} \rightarrow A_f$, $\phi \rightarrow CN$, $l_{sp} \rightarrow t_{n,m}$) which incorporate material parameters chosen to fit experimental data. The latter category of edges provide opportunities for researchers to propose hand-crafted constitutive relations of different degrees of complexities. For example, their forms can be linear, quadratic, exponential functions or be approximated by artificial neural networks (ANNs). For illustration purposes, we consider a simple digraph of traction-separation models involving only the nodes $\{\delta, t, \delta_{n,m}, t_{n,m}, \phi, CN, A_f\}$. Figure 2 provides examples of two admissible and two illegal digraph configurations according to the Rules 1-5.

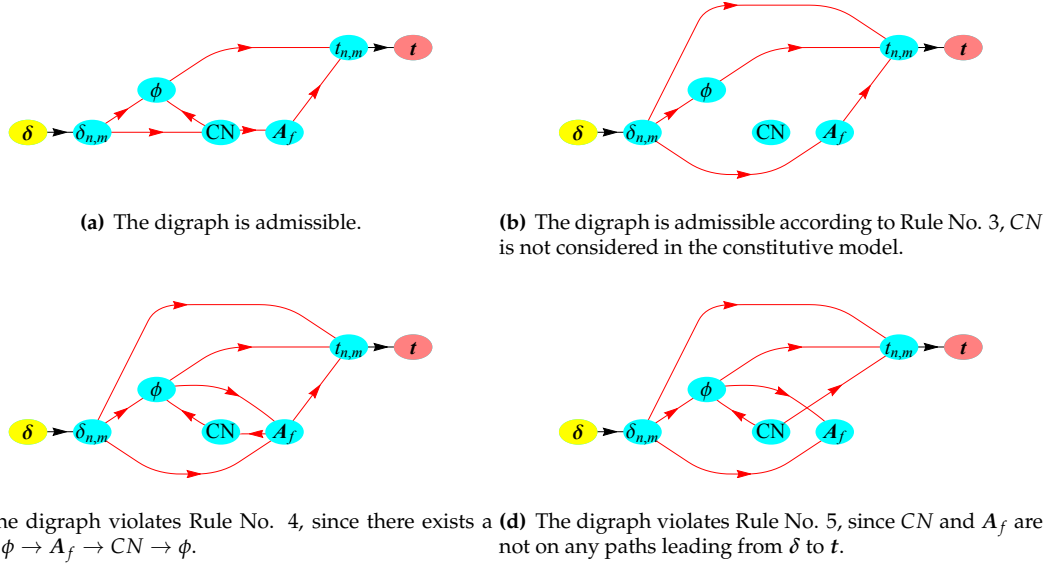


Figure 2: Examples of admissible directed graphs (a-b) and illegal directed graphs (c-d) representing information flow in traction-separation models involving internal physical quantities of porosity ϕ , coordination number CN and fabric tensor A_f . The yellow node of separation δ refers to the root node, the pink node of traction t refers to the leaf node, and the cyan nodes refer to intermediate nodes. The black arrows refer to "definition" or "universal principles" edges. The red arrows refer to "phenomenological relations" edges.

3 Score system for model evaluation and objective function

A score system must be introduced to evaluate the generated directed graphs for constitutive models such that the accuracy and credibility in replicating the mechanical behavior of real-world materials can be assessed. This score system may also serve as the objective function that defines the rewards for the deep reinforcement learning agent to improve the generated digraphs and resultant constitutive laws. In this work, we define the score as a positive real-valued function of the range $[0, 1]$ which depends on the measures A_i ($i = 1, 2, 3, \dots, n$) of n important features of a constitutive model,

$$\text{SCORE} = F(A_1, A_2, A_3, \dots, A_n), \quad (3)$$

where $0 \leq A_i \leq 1$. Some features are introduced to measure the performance of a model such as the accuracy and computation speed. Other features are introduced to enforce constraints to ensure the admissibility of a constitutive model, such as the frame indifference and the thermodynamics consistency. Suppose there are n_{pfm} measures of performance features A_i^{pfm} and n_{crit} measures of critical features A_i^{crit} in the measure system of constitutive models, the score takes the form,

$$\text{SCORE} = \left(\prod_{j=1}^{n_{\text{crit}}} A_j^{\text{crit}} \right) \cdot \left(\sum_{i=1}^{n_{\text{pfm}}} w_i A_i^{\text{pfm}} \right), \quad (4)$$

where $w_i \in [0, 1]$ is the weight associated with the measure A_i^{pfm} , and $\sum_{i=1}^{n_{\text{pfm}}} w_i = 1$. In this section, two examples of measures of accuracy A_{accuracy} and prediction consistency $A_{\text{consistency}}$ are presented.

3.1 Accuracy of calibrations and forward predictions

In this work, the abilities of the models to replicate calibration data and make forward predictions are considered separately. Here we introduce a cross-validation procedure in which the dataset used for training the models (e.g. identifying material parameters (e.g. Wang et al. [2016], Liu et al. [2016a]) or adjusting weights of neurons in recurrent neural networks (e.g. Lefik and Schrefler [2002], Wang and Sun [2018])) is mutually exclusive to the testing dataset used to evaluate the quality of blind predictions. The details of the generation of these calibration and testing data sets using frictional discrete element simulations are presented in Appendix A. Both calibration and blind prediction results are compared against the target data. The mean squared error (MSE) commonly used in statistics and also as objective function in machine learning is chosen as the error measure for each data sample i in this study, i.e.,

$$\text{MSE}_i = \frac{1}{N_{\text{feature}}} \sum_{j=1}^{N_{\text{feature}}} [\mathcal{S}_j(Y_{ij}^{\text{data}}) - \mathcal{S}_j(Y_{ij}^{\text{model}})]^2, \quad (5)$$

where Y_{ij}^{data} and Y_{ij}^{model} are the values of the j th feature of the i th data sample, from target data value and predictions from constitutive models, respectively. N_{feature} is the number of output features. \mathcal{S}_j is a scaling operator (standardization, min-max scaling, ...) for the output feature $\{Y_{ij}\}$, $i \in [1, N_{\text{data}}]$.

The empirical cumulative distribution functions (eCDFs) are computed for MSE of the entire dataset $\{\text{MSE}_i\}$, $i \in [1, N_{\text{data}}]$, for MSE of the training dataset $\{\text{MSE}_i\}$, $i \in [1, N_{\text{traindata}}]$ and for MSE of the test dataset $\{\text{MSE}_i\}$, $i \in [1, N_{\text{testdata}}]$, with the eCDF defined as [Kendall et al., 1946],

$$F_N(\text{MSE}) = \begin{cases} 0, & \text{MSE} < \text{MSE}_1, \\ \frac{r}{N}, & \text{MSE}_r \leq \text{MSE} < \text{MSE}_{r+1}, \quad r = 1, \dots, N-1, \\ 1, & \text{MSE}_N \leq \text{MSE}, \end{cases} \quad (6)$$

where $N = N_{\text{data}}$, or $N_{\text{traindata}}$, or N_{testdata} , and all $\{\text{MSE}_i\}$ are arranged in increasing order. A measure of accuracy is proposed based on the above statistics,

$$A_{\text{accuracy}} = \max\left(\frac{\log[\max(\varepsilon_{P\%}, \varepsilon_{\text{crit}})]}{\log \varepsilon_{\text{crit}}}, 0\right), \quad (7)$$

where $\varepsilon_{P\%}$ is the P th percentile (the MSE value corresponding to $P\%$ in the eCDF plot) of the eCDF on the entire, training or test dataset. $\varepsilon_{\text{crit}} \ll 1$ is the critical MSE chosen by users such that a model can be considered as "satisfactorily accurate" when $\varepsilon_{P\%} \leq \varepsilon_{\text{crit}}$.

3.2 Consistency of accuracy between calibrations and forward predictions

For the examination of the consistency in model predictions on training data and test data, the K-sample Anderson-Darling (AD) test of goodness-of-fit (gof) is conducted to check whether the eCDFs of training and test data come from the same probability distribution, while this distribution is unspecified [Anderson and Darling, 1954, Scholz and Stephens, 1987]. It is a non-parametric hypothesis test and determines whether the null hypothesis H_0 that the two eCDFs come from the same continuous distribution can be rejected or not, under a chosen significance level α_{gof} . The method consists of calculating a normalized AD test statistic, critical values of the AD statistic that depends on the sample sizes, and a p -value indicating the approximated significance level at which H_0 can be rejected. If the p -value is smaller than the significance level α_{gof} , the H_0 hypothesis is rejected. Otherwise there is insufficient evidence to reject H_0 . In this work, we define the following binary measure for the consistency of the MSE distributions, with the significance level α_{gof} ,

$$A_{\text{consistency}} = H^{\alpha_{\text{gof}}} = \begin{cases} 0, & p\text{-value} < \alpha_{\text{gof}}, \\ 1, & p\text{-value} \geq \alpha_{\text{gof}}. \end{cases} \quad (8)$$

4 Game of the traction-separation law

Our focus in this paper is primarily on the meta-modeling game invented for generating traction-separation models. Nevertheless, similar games can be defined for generating other types of constitutive models based on the ideas presented in this work. With the directed graph representations of traction-separation models as presented in Section 2, the process of developing a model can be recast as a game of making a sequence of decisions in generating edges between nodes in the digraphs. The player of the game can be a human or an AI agent. The game starts with an initial "game board" of digraph with predefined nodes and no edge formed between them. Each step of the game consists of activating only one edge among all possible choices of edges in the predefined action space, following the predefined rules of the game. The game terminates when a complete and admissible digraph following the rules in Section 2 is established. The output models of the game are measured by a score system as presented in Section 3.

The game can be mathematically formalized as a Markov decision process. The human or AI agent observes the state of the game s_t at the current step t from the game environment (the directed graph that represents a constitutive model) in the form of a vector of binaries indicating the on/off status of each valid edge choices in the action space. The agent takes an action a_t on the game environment in the form of an integer indicating the next edge to switch on in the action space. The action a_t is sampled from a vector of probabilities $\pi(s_t)$ of taking each valid action from the state s_t . Consequently, the state of the game becomes s_{t+1} at the next step $t + 1$. The agent also receives a reward r_{t+1} for the action a_t of taking the game state from s_t to s_{t+1} . Each policy applied in a complete gameplay produces a particular trajectory $s_0, a_0, r_1, s_1, a_1, r_2, \dots, a_{t-1}, r_t, s_t, a_t, \dots, a_{T-1}, r_T, s_T$. Once a complete constitutive model is generated, the model score is evaluated. The final reward r_T is defined as: if the current score is higher than the average score of models from a group of already played games by the

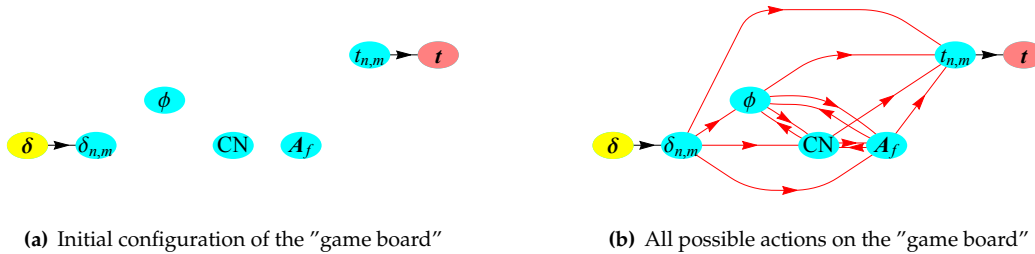


Figure 3: A game of traction-separation model for the digraph example in Figure 2. (a) the initial "board" on which the game is played. (b) All possible actions for picking the edges connecting the nodes are represented by the red arrows.

Environment	Benchmark training and test data, idealized multigraph for constitutive models
Agent	Human or AI
State s	A list of binaries indicating the on/off status of each valid edge choice
Action a	An integer indicating the next edge to switch on from the current game state
Reward r	Win (1) / loss (-1) according to the score of the constitutive model in Section 3
$\pi(s, a)$	Probability of taking action a at state s
$v(s)$	Expected reward of state s
Q-value $Q(s, a)$	Expected reward from taking action a at state s

Table 1: Key ingredients of the game of constitutive models in directed graph.

agent, then the current game wins and $r_T = 1$, otherwise, the current game loses and $r_T = -1$. The average score can be initialized to 0 for the first game.

Note that the reward is only available at the end of the game, similar to the game of Chess and Go. r_T is known according to the score of the generated model. The previous rewards $r_{t < T}$, however, can only be estimated. For a human agent, both rewards $r_{t < T}$ and move probabilities $\pi(s)$ come from "intuition" gained during many constitutive modeling practices. An experienced human modeler estimates the rewards and probabilities more accurately and hence more likely generates better constitutive models. For an AI agent, $r_{t < T}$ and $\pi(s)$ are approximated by hand-crafted mathematical functions or recently neural networks as in deep reinforcement Q-learning. They are estimated based on the expected game reward of taking action a from state s (Q-value) $Q(s, a)$ and the value of current state $v(s)$. The above-mentioned important quantities for mathematical descriptions of the gameplays are summarized in Table 1. Moreover, the constitutive modeling game is compared side-by-side with the game of Chess more familiar to the public in Table 2, in the aspects of the board to play on, the permitted actions to execute, the criteria for winning the game, etc.

For illustration purposes, we provide a simple game example for the digraph presented in Figure 2, which only involves the nodes $\{\delta, t, \delta_{n,m}, t_{n,m}, \phi, CN, A_f\}$. Figure 3 presents the "initial game board" and all possible edges choices in the current game definition. The configuration of the digraph, or the state of the game, can be totally described by a list of binaries for 13 edges $[\delta_{n,m} \rightarrow \phi, \delta_{n,m} \rightarrow CN, \delta_{n,m} \rightarrow A_f, \delta_{n,m} \rightarrow t_{n,m}, \phi \rightarrow CN, \phi \rightarrow A_f, \phi \rightarrow t_{n,m}, CN \rightarrow \phi, CN \rightarrow A_f, CN \rightarrow t_{n,m}, A_f \rightarrow \phi, A_f \rightarrow CN, A_f \rightarrow t_{n,m}]$ (The edges $\delta \rightarrow \delta_{n,m}$ and $t_{n,m} \rightarrow t$ are definitions and always active). The list also represents the entire action space. The action a is an integer $\in [0, 12]$ indicating the next edge ID to activate in the list. The legal moves at the current game state are represented by a list of 13 binaries indicating whether the corresponding edges are allowed to be activated for the next action step. The rule of the legal moves are as follows: (1) if one edge has already been selected, it is excluded from the selection of actions; (2) if an edge between two intermediate nodes has been selected, the other edge involving these two nodes but with opposite direction is also excluded (e.g.,

	Game of Chess	Game of constitutive modeling in directed graph
Definition of game	Make a sequence of decisions to maximize the probability to win	Make a sequence of decisions to maximize the score of the constitutive model
Game board	8×8 grid	Directed graph with predefined nodes of physical quantities and edges of definition or universal principles
Game state	Configuration of chess pieces on the board	Configuration of directed graph representing the constitutive model
Game action	Move chess pieces	Select among modeling choices. For instance <ul style="list-style-type: none"> 1. What physical quantities are included? 2. How physical quantities are linked? 3. What are the edges between physical quantities?
Game rule	Restrictions on chess piece movements	Universal principles Rules in Section 2 Specific restrictions on edge choices
Game reward	Win, draw or loss (discontinuous)	Win or loss (discontinuous) from comparison of model scores (continuous)
Reward evaluation	Only available at the end	Only available at the end

Table 2: Comparison of the essential definitions between the game of Chess and the game of constitutive modeling in directed graph.

The edges $\phi \rightarrow CN$ and $CN \rightarrow \phi$ are mutually exclusive); (3) the resultant digraph must obey the rules in Section 2. Figure 4 provides a gameplay example of the constitutive modeling game in Figure 3, with mathematical representations of game states, actions and legal actions, as well as the Markov decision process.

The score evaluation (Section 3) requires model calibration on training data, and forward predictions on test data. The procedure for score evaluation is as follows. Once the final digraph configuration is determined, all paths (information flows) leading from δ to t and all predecessors for each node in the paths are identified using the graph theory (software package NetworkX). Secondly, the predecessor nodes for the terminal node t within these paths are identified. Recursively going upstream along all the information flows, the predecessors for these nodes are identified, until the final predecessor node is the start node δ only. All the predecessor-successor node pairs can be connected by either mathematical equations frequently used in handcrafted constitutive models (linear, quadratic, exponential, power law, etc.) or artificial neural networks. In this work, we take the advantage of the flexibility of ANNs that they are universal function approximators to continuous functions of various complexity on compact subsets of R^n (Universal approximation theorem, [Hornik et al., 1989]). Moreover, a special type of ANN, recurrent neural network (e.g., long short-term memory LSTM [Hochreiter and Schmidhuber, 1997], gated recurrent units GRU [Cho et al., 2014, Chollet et al., 2015]), can capture the function of a time series of inputs, which is ideal for replicating the path-dependent material behavior. Hence, we only focus on ANN edges, without loss of generality of the meta-modeling games. The hybridized constitutive models with both mathematical

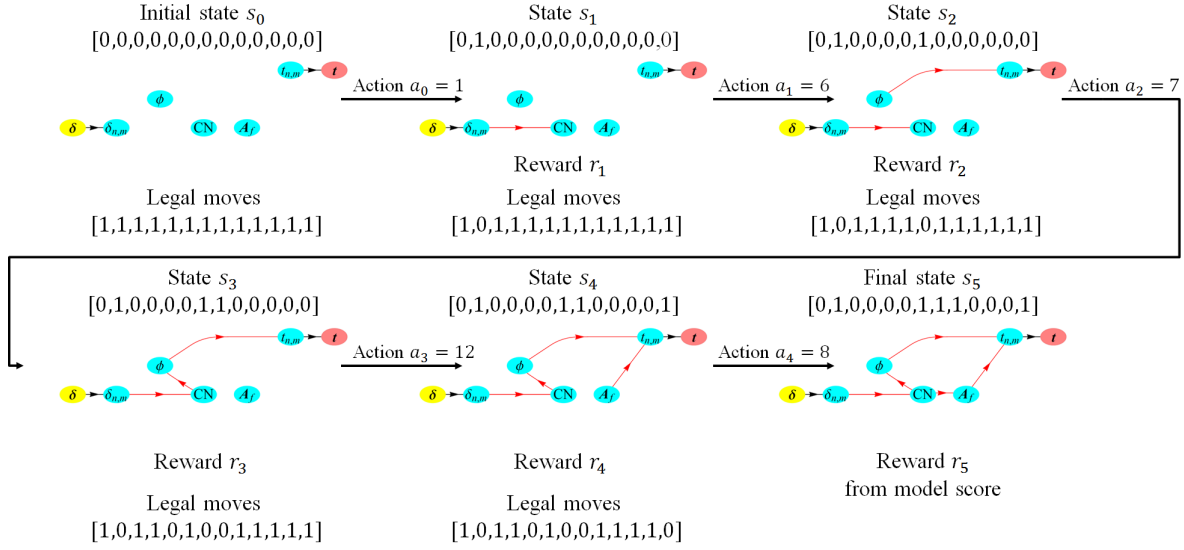


Figure 4: A gameplay example formalized as a Markov decision process $(s_0, a_0, r_1, s_1, a_1, r_2, s_2, a_2, r_3, s_3, a_3, r_4, s_4, a_4, r_5, s_5)$ for the digraph game in Figure 3. The states are lists of binaries for 13 edges $[\delta_{n,m} \rightarrow \phi, \delta_{n,m} \rightarrow CN, \delta_{n,m} \rightarrow A_f, \delta_{n,m} \rightarrow t_{n,m}, \phi \rightarrow CN, \phi \rightarrow A_f, \phi \rightarrow t_{n,m}, CN \rightarrow \phi, CN \rightarrow A_f, CN \rightarrow t_{n,m}, A_f \rightarrow \phi, A_f \rightarrow CN, A_f \rightarrow t_{n,m}]$. The actions a are integers $\in [0, 12]$ (the list indices start from 0) indicating the next edge ID to activate. The legal moves are lists of binaries indicating whether the edges are allowed to be activated next. Final reward r_5 is determined by the model score evaluated at the end of the game. r_{1-4} are only estimated by “intuitions” on whether the current policy can lead to a win or not, until r_5 is known. Note that the Markov decision process leading to the final digraph configuration s_5 is not unique.

equation edges and ANN edges will be studied in a separate research. The predecessor-successor node pairs are also inputs and outputs of all ANNs involved in the constitutive model. For example, there are two paths in the final digraph s_5 in Figure 4: $\{\delta \rightarrow \delta_{n,m} \rightarrow CN \rightarrow A_f \rightarrow t_{n,m} \rightarrow t\}$ and $\{\delta \rightarrow \delta_{n,m} \rightarrow CN \rightarrow \phi \rightarrow t_{n,m} \rightarrow t\}$. Then the three required ANNs are, represented as input-output pairs, $[\delta_{n,m} \rightarrow CN]$, $[CN \rightarrow \phi, A_f]$ and $[\phi, A_f \rightarrow t_{n,m}]$. The parameters in each ANN are calibrated with training data of the input and output features using back propagations. The final output of t is predicted by executing consecutively the ANNs following the established paths from δ to t in the directed graph. In the numerical examples of this paper, the same neural network architecture is used for all ANNs: two hidden layers of 32 GRU neurons in each layer, and the output layer is a dense layer with linear activation function. All input and output data are preprocessed by standard scaling using mean values and standard deviations [Pedregosa et al., 2011]. Each input feature considers its current value and 19 history values prior to the current loading step. Each ANN is trained for 1000 epochs using the Adam optimization algorithm [Kingma and Ba, 2014], with batch size of 256.

5 Deep reinforcement learning for generating constitutive laws

With the game of constitutive modeling completely defined, a deep reinforcement learning (DRL) algorithm is employed as a guidance of taking actions in the game to maximize the final model score (Figure 5). This tactic is considered one of the key ideas leading to the major breakthrough in AI playing the game of Go (AlphaGo Zero) [Silver et al., 2017b], Chess and shogi (Alpha Zero) [Silver et al., 2017a] and many other games. The learning is completely free of human interventions. It does not need previous human knowledge in traction-separation model as a starter database. The AI agent

simply learns to improve from a number of games it played and from the corresponding model scores and game rewards, even if the initially generated digraph configurations make very little sense for a traction-separation model. Moreover, during the self-plays and training, no human guidance is needed.

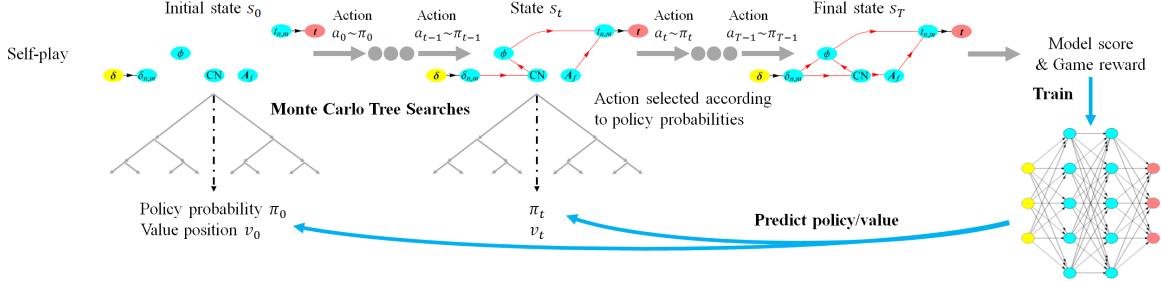


Figure 5: Self-play reinforcement learning of traction-separation law.

A (deep) neural network f_θ with parameters θ (weights, bias, ... of the artificial neurons) takes in the current configuration of the directed graph of the constitutive law s and outputs a policy vector \mathbf{p} with each component $p_a = p(s, a)$ representing the probability of taking the action a from state s , as well as a scalar v estimating the expected score of the constitutive law game from state s , i.e.,

$$(\mathbf{p}, v) = f_\theta(s). \quad (9)$$

These outputs from the policy/value network guide the game play from the AI agent.

At each state s , the action to take is sampled from an action probability $\pi(s)$. This probability is based on the policy \mathbf{p} predicted from the neural network enhanced by a Monte Carlo Tree Search (MCTS) ([Browne et al., 2012]). The search tree is composed of nodes representing states s of the game, and edges representing permitted actions a from s . Each edge (s, a) possesses a list of statistics $[N(s, a), W(s, a), Q(s, a)]$, where $N(s, a)$ is the number of visits to the edge during MCTS search, $W(s, a)$ is the total action value and $Q(s, a) = \frac{W(s, a)}{N(s, a)}$ is the mean action value. The search procedure consists of firstly a recursive selection of a sequence of optimal actions a^0, a^1, a^2, \dots leading to the corresponding child states s^1, s^2, s^3, \dots , starting from the root state s^0 , until a leaf node of state s^l (that has never been encountered before in the search) is reached. The criteria for selection from a state s is that the action a maximizes the upper confidence bound $U(s, a)$ of the Q-value, among all valid actions. The upper bound is defined as

$$U(s, a) = Q(s, a) + U_Q(s, a) = Q(s, a) + c_{puct} p(s, a) \frac{\sqrt{\sum_b N(s, b)}}{1 + N(s, a)}. \quad (10)$$

where c_{puct} is a parameter controlling the level of exploration. If s^l is not a terminal state that ends the game, then its $\mathbf{p}(s^l)$ and $v(s^l)$ are predicted from the policy/value neural network $f_\theta(s^l)$. The search tree is expanded and the statistics for each edge (s^l, a) is initialized to $[N(s, a) = 0, W(s, a) = 0, Q(s, a) = 0]$. Otherwise, $v(s^l)$ is equal to the final reward of the constitutive modeling game. Finally, $v(s^l)$ is propagated back to the parent states $\{s^0, s^1, s^2, \dots, s^l\}$ and actions $\{a^0, a^1, a^2, \dots, a^{(l-1)}\}$ traversed during the search. Their statistics are updated as

$$N(s^i, a^i) = N(s^i, a^i) + 1, \quad W(s^i, a^i) = W(s^i, a^i) + v(s^l), \quad Q(s^i, a^i) = \frac{W(s^i, a^i)}{N(s^i, a^i)}, \quad \text{for all } i < l. \quad (11)$$

The MCTS procedure is repeated a number of times. The searches in MCTS eventually yield a vector of search probabilities $\pi(s^0)$ recommending actions to take from the root position s^0 . $\pi(s^0)$ is

proportional to the exponentiated visit count for each edge, i.e.,

$$\pi(s^0, a) = \frac{N(s^0, a)^{-\tau}}{\sum_b N(s^0, b)^{-\tau}}, \quad (12)$$

where τ is a positive temperature parameter that also controls the level of exploration. The MCTS algorithm for the game of constitutive models is illustrated in Figure 6.

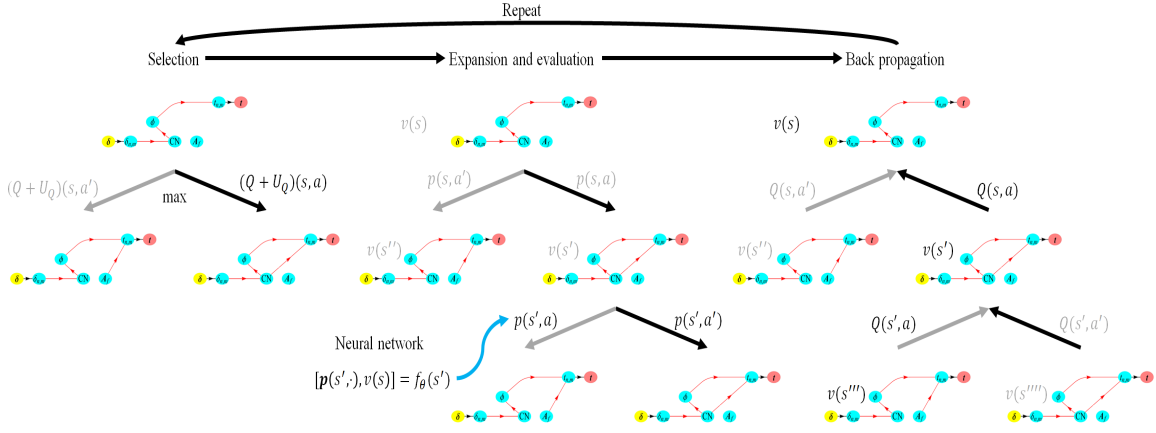


Figure 6: Monte Carlo Tree Search (MCTS) in a game of constitutive models (figure design adopted from [Silver et al., 2017b]). A sequence of actions are selected from the root state s^0 , each maximizing the upper confidence bound $Q(s, a) + U_Q(s, a)$. The leaf node s^l is expanded and its policy probabilities and position value are evaluated from the neural network $(p(s^l), v(s^l)) = f_\theta(s^l)$. The action values Q in the tree are updated from the evaluation of the leaf node. Finally the search probability $\pi(s^0)$ for the root state s^0 is returned to guide the next action in self-play.

During one episode of self-play by the AI agent, the above MCTS algorithm is executed for each state s_t in the sequence of encountered states $\{s_0, s_1, s_2, \dots, s_{T-1}\}$. The root node s^0 of the search tree is set to s_t as the game progresses to the state s_t . All child nodes and their statistics constructed in the MCTS for the prior game states are preserved. The training data for the neural network consists of (s_t, π_t, z_t) obtained from a number of full plays of the constitutive law game guided by the aforementioned reinforcement learning algorithm. π_t is the estimation of policy after performing MCTS from state s_t and z_t is the reward of the generated constitutive model at the end of the game s_T . The loss function to be minimized by adjusting parameters θ using back propagation is,

$$l = \sum_t (v(s_t) - z_t)^2 + \sum_t \pi_t \log[p(s_t)], \quad (13)$$

which is the combination of mean squared errors in game reward (1 or -1) and cross-entropy losses in policy probabilities. Hence, accordingly, the activation functions for the output layer are the hyperbolic tangent function $\tanh(x) = \frac{e^{2x} - 1}{e^{2x} + 1}$ and the softmax function [Nasrabadi, 2007]. The procedure of DRL guided self-plays and the following training of the network f_θ is iterated until the score of the generated directed graph of the constitutive model does not improve.

6 Numerical Experiments and Applications

In this section, we present two traction-separation modeling games with different digraph complexities to demonstrate the intelligence, robustness and efficiency of the deep reinforcement learning

algorithm on improving the accuracy and consistency of the generated traction-separation models through self-plays. In both examples, sub-scale discrete element simulations (DEM) are used to generate synthetic benchmark data for model calibrations and blind prediction evaluations. The procedure of database generation from a pre-consolidated representative volume element (RVE) of a frictional contact material is described in Appendix A. The third numerical example presents a multiscale finite element simulation where the previously auto-generated optimal model is used as a scale-bridging constitutive model for pre-existing interface.

6.1 Numerical Experiment 1: Determining optimal physical relationships for traction-separation laws

In the first example, our goal is to test the DRL algorithm and see whether it can determine the optimal topological relations among microstructural physical quantities of porosity ϕ , coordination number CN and fabric tensor A_f . In Wang and Sun [2018], the authors use domain expertise, i.e., knowledge from previous literature on fabric tensor and critical state theory to deduce that the porosity and fabric tensor can be used as state variables to improve the forward prediction accuracy of the traction-separation law (cf. Fu and Dafalias [2011], Li and Dafalias [2011], Sun [2013], Wang and Sun [2016]). In this work, we do not make any assumption or introduce any interpretation to the meta-modeling computer agent. Instead, we simply make a number of physical quantities measured from discrete element simulations available as vertices in the directed graph but do not introduce any relation (edge) manually. In other words, the edge set that represents the relations of the physical quantities is self-discovered by the computer agent from the reinforcement learning without any human intervention. We document our training procedure and analyze the performance of the models generated by the meta-modeling approach.

The directed graphs, states, actions, rewards and game rules of the modeling game have been defined in Sections 2 and 4, and illustrated in Figures 2, 3 and 4. The action space is of dimension 13. Through exhaustive plays of the game, the authors count 3200 possible game states, among which 591 states represent complete and admissible directed graph configurations according to the game rules. The model score is defined as:

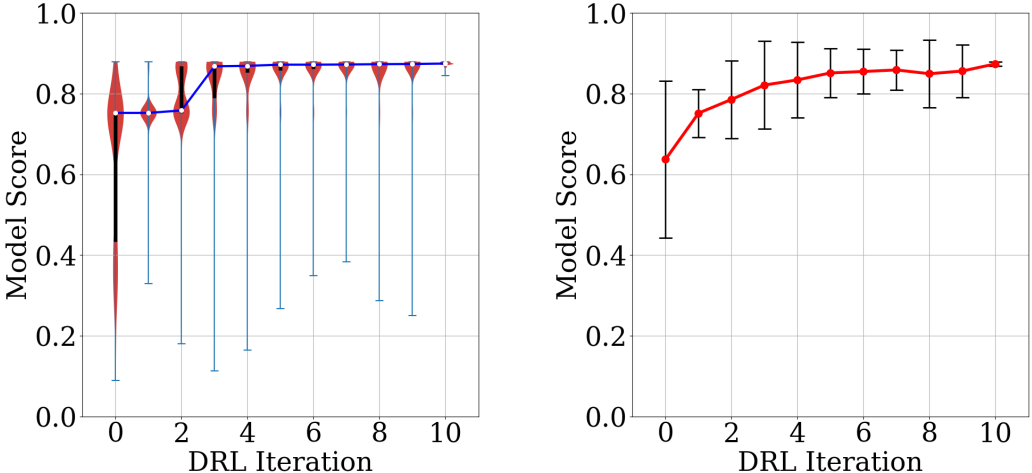
$$\text{SCORE} = 0.45 * A_{\text{accuracy}}^{\text{calibration}} + 0.45 * A_{\text{accuracy}}^{\text{prediction}} + 0.1 * A_{\text{consistency}}, \quad (14)$$

where $P\% = 90\%$ and $\epsilon_{\text{crit}} = 1e^{-6}$ for accuracy evaluations and $\alpha_{\text{gof}} = 1\%$ for consistency evaluations. The training data for model calibration contains 50 loading cases, and the test data for forward prediction evaluation contains 150 loading cases.

The DRL meta-modeling procedure contains 10 iterations of "exploration and exploitation" of game strategies, by setting the temperature parameter τ to 1. Then an iteration of "competitive gameplay" ($\tau = 0.01$) is conducted to showcase the performance of the final trained AI agent. Each iteration consists of 20 self-plays of the game. Each game starts with a randomly initialized neural network for the policy/value predictions, and each play step require 20 MCTS simulations. Then the play steps and corresponding final game rewards are append to the set of training examples for the training of the policy/value network. Due to the randomness of the initialized neural network and the MCTS search for each play step, each run of the DRL algorithm may yield different game play results, concerning the starting game policy, the speed of improvement, and the converged optimal policy. In this numerical example, the DRL procedure is repeated 20 times and all model scores that the AI agent played during the iterations are recorded. Hence for each iteration, there are 400 gamplays for statistical analysis (20 gamplays X 20 repeated procedures). The gameplay results are presented in Figure 7.

At the first DRL iteration, the AI agent only knows the rule of the game without human knowledge on neither which physical quantities are essential in predicting the tractions nor how they should be connected. The AI just plays with trial-and-error following strategies guided by random initial neural network and MCTS. This lack of gameplay knowledge can be seen from the widely spread density

distribution of model scores between maximum and minimum scores, large interquartile range between 25% and 75%, and the large standard deviation (Figure 7). In the subsequent iterations, the AI plays with increasing knowledge of game play reinforced by the ultimate game rewards, and it shows intelligence in keep playing games with better outcomes. This is shown by the increase in median and average of scores, the narrowing of interquartile range and the migration of the density distribution towards higher scores. The automatic learning is very efficient. Statistically, after 5 iterations (100 games out of the total 591 possible game outcomes), the scores already concentrate around the maximum. Few bad games could be played, since the AI is still allowed to explore different game possibilities to avoid convergence to local maximum. The strength of the AI agent after 10 iterations is tested by suppressing the "exploration plays", and the outcome game scores show outstanding performances. Figure 8 illustrates the improvement of knowledge of traction-separation constitutive modeling by four representative digraph games played during the DRL iterations. The traction predictions from the resultant constitutive models are compared against both training data and unseen test data. In addition, five examples of blind predictions from the optimal digraph configuration (the 4th digraph in Figure 8) obtained in this game are shown in Figure 9.



(a) Violin plots of the density distribution of model scores in each DRL iteration (b) Mean value and \pm standard deviation of model score in each DRL iteration

Figure 7: Statistics of the model scores in deep reinforcement learning iterations from 20 separate runs of the DRL procedure for Numerical Experiment 1. Each DRL procedure contains ten iterations 0-9 of "exploration and exploitation" (by setting the temperature parameter $\tau = 1.0$) and a final iteration 10 of "competitive gameplay" ($\tau = 0.01$). Each iteration consists of 20 games. (a) Violin Plot of model scores played in each DRL iteration. The shade area represents the density distribution of scores. The white point represents the median. The thick black bar represents the interquartile range between 25% quantile and 75% quantile. The maximum and minimum scores played in each iteration are marked by horizontal lines. (b) Mean model score in each iteration and the error bars mark \pm standard deviation.

6.2 Numerical Experiment 2: Data-driven discovery for enhancement of traction-separation laws

In the second example, we consider another common scenario in which we attempt to convert qualitative observations into quantitative predictions with the help of the reinforcement learning algo-

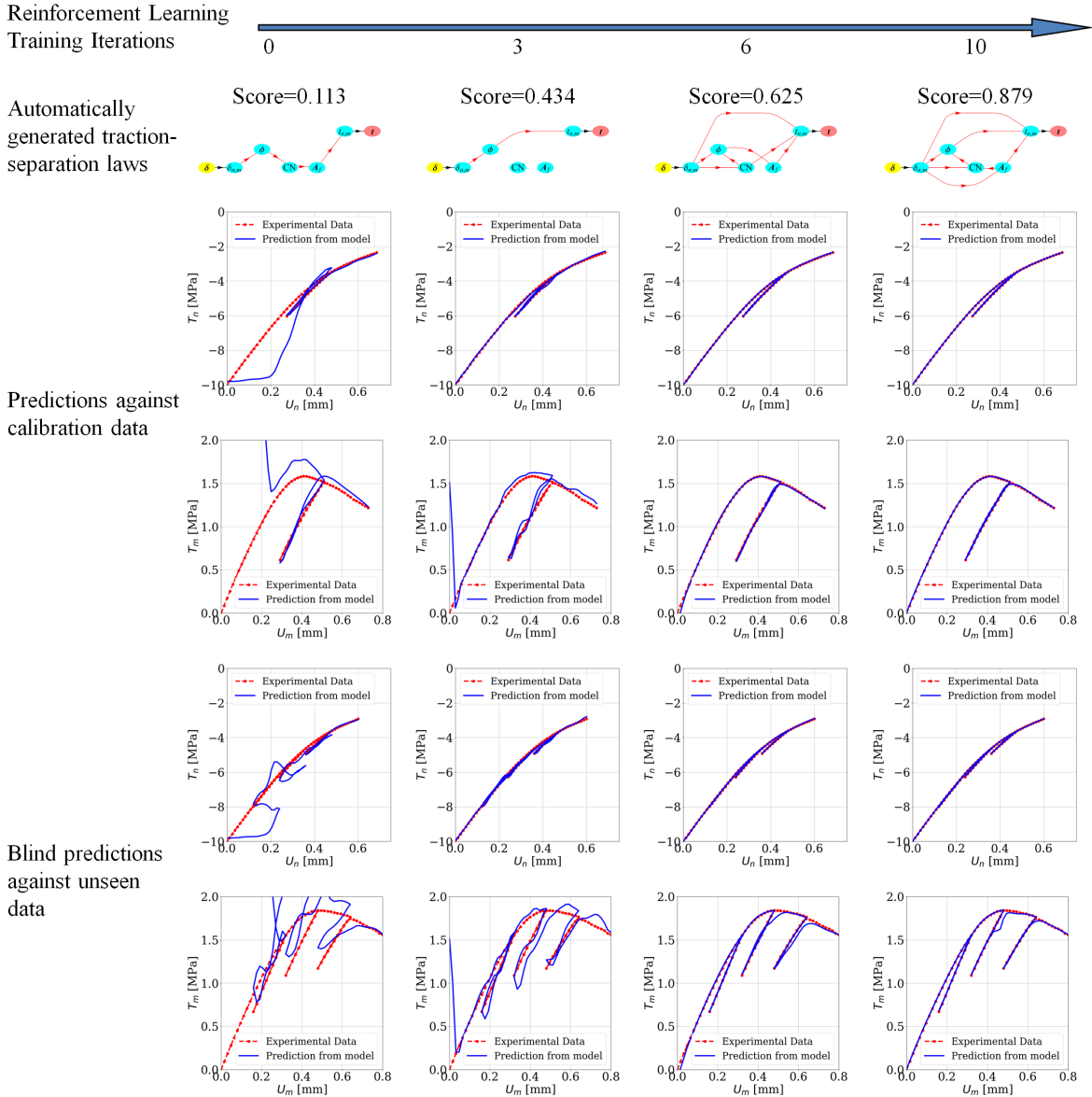


Figure 8: Knowledge of directed graphs of traction-separation models learned by deep reinforcement learning in Numerical Experiment 1. Four representative digraph games played during the DRL iterations and their prediction accuracy against training and test data are presented.

rithm as a tool for augmented intelligence. The need to interpret observations of mechanisms into predictions is one of the oldest problems in constitutive modeling [Pastor et al., 2011]. For instance, the observation that yielding depends on the amount of normal traction leads to the Mohr-Coulomb yield criterion [Timoshenko, 1953]. The evolution of fabric tensor has been incorporated into the hardening law and the plastic flow rule to capture the induced anisotropy and critical state of sand [Mehrabadi et al., 1982, Dafalias and Manzari, 2004, Dafalias et al., 2004]. However, recent advancements on the application of graph theory as well as the experimental techniques such as micro-CT imaging have revealed many geometric measures on the grain connectivity that help explaining the onset of shear band [Tordesillas et al., 2011, 2010], coherent vortex structure [Williams and Rege, 1997]

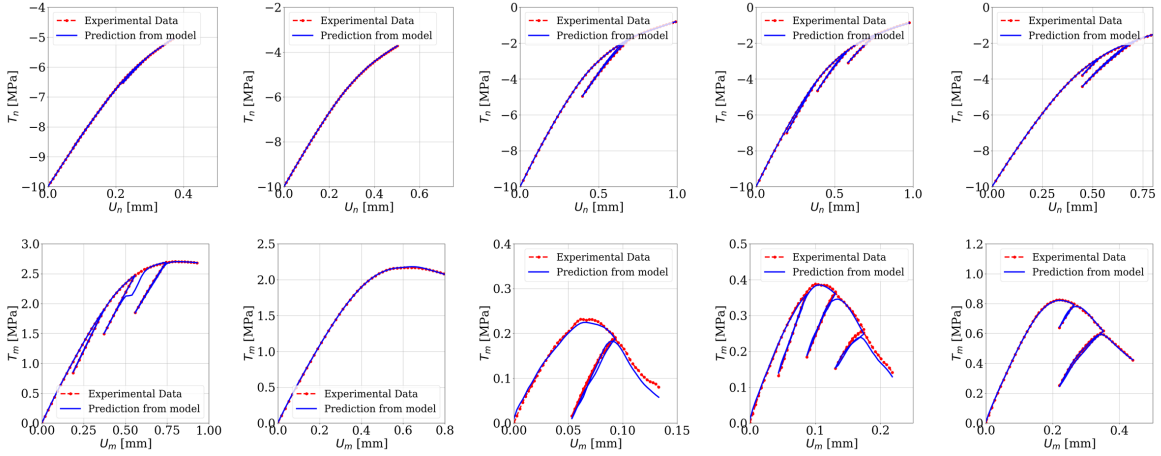


Figure 9: Five examples of blind predictions from the optimal digraph configuration (the 4th digraph in Figure 8) against unseen data among test database of 150 loading cases.

and post-bifurcation behaviors in granular materials [Sun et al., 2013a, Wang and Sun, 2015, Liu et al., 2018]. While these discoveries of new knowledge are indeed encouraging, one cannot make use of them without investing significant efforts and time to derive, verify, and validate new constitutive laws that incorporate those new information. Hence the graph-theoretical approaches, although have found great promises on analyzing the granular assemblies obtained from real or virtual experiments, have not yet made significant impacts on constitutive laws used for engineering applications. Our meta-modeling approach is capable of overcoming this bottleneck by efficiently automating some of these tasks currently undertaken by modelers. This second numerical experiment is used to demonstrate how the augmented intelligence can be used to incorporate the insights from observations into predictions without manually re-writing an existing constitutive law every time new information comes up.

This example is an extension of the first numerical experiment, in which more microstructural information are considered, including the fabric of strong interactions A_{sf} and four measures of grain connectivities d_a , c_t , l_{sp} , ρ_g . The task of identifying their roles in constitutive models for granular materials is now simply recast as defining a new game with augmented vertex set in digraph and extended action space. The "game board" and all possible actions for this new game are shown in Figure 10. The dimension of the action space increases from 13 to 71. A particular game rule is added to test the flexibility of the DRL algorithm in handling different types of game constraints: the strong fabric tensor A_{sf} and the fabric tensor A_f , since both are geometric measures of inter-particles forces, are mutually exclusive in the final digraphs of constitutive models. The number of possible game states increases from 3200 to over 400000. The number of complete and admissible directed graph configurations increases from 591 to over 20000. The score definition is the same as Equation (14). The meta-modeling algorithm try to learn the optimal ways to incorporate the microstructural information to make better predictions only from the training database of 50 loading cases, while the gained knowledge is validated on the test database of another 150 loading cases. The parameters for the DRL meta-modeling algorithm are set as: 10 iterations of "exploration and exploitation", 1 iteration of "competitive gameplay", 30 self-plays in each iteration, and 30 MCTS simulations in each play step.

The statistics of the gameplay results from 5 separate runs of the DRL procedure are presented in Figure 11. We observe a very efficient improvement in generated traction-separation models, even though the number of legal game states in the new game has largely increased. Figure 12 exhibits four representative digraph configurations developed during DRL iterations, as well as their prediction

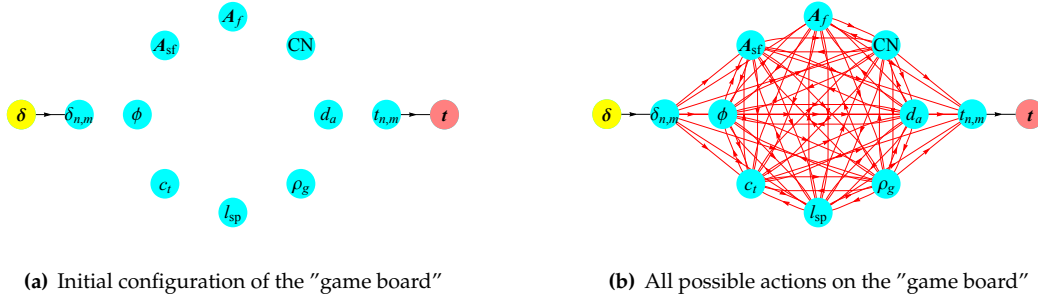


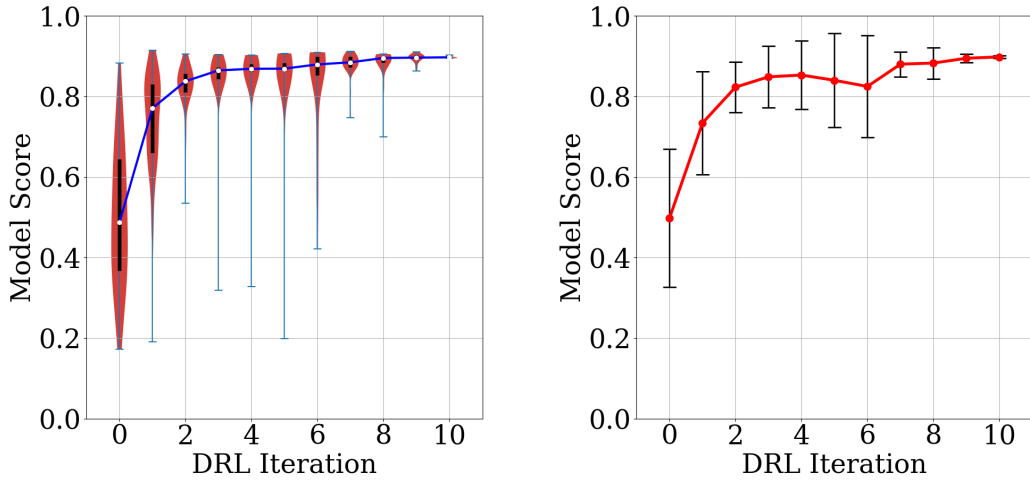
Figure 10: A game of traction-separation model for a digraph involving the nodes $\{\delta_{n,m}, t_{n,m}, \phi, CN, A_f, A_{sf}, d_a, c_t, l_{sp}, \rho_g\}$ (detailed in Section 2). (a) the initial "board" on which the game is played. (b) All possible actions for picking the edges connecting the nodes are represented by the red arrows.

quality on calibration data and unseen data. It can be seen that the information flows in a constitutive model are of crucial importance. Although the first and the fourth graphs both incorporate the same types of microstructural information, the difference in the ways how these information are connected results in significant difference in model scores of 0.191 and 0.915, respectively. Moreover, the DRL algorithm develops the intelligence of selecting the strong fabric tensor A_{sf} over the fabric tensor A_f in order to further improve the prediction score of the model. Five blind prediction examples of the optimal digraph configuration (the 4th digraph in Figure 12) obtained in this game are presented in Figure 13. Comparing to the numerical example 1 (Figure 9), the augmented knowledge of additional microstructural information in constitutive models lead to more accurate representations of granular materials.

6.3 Application: Multiscale bridging using DRL-generated traction-separation model in finite element modeling

In this example, we demonstrate that the traction-separation model auto-generated by the proposed DRL meta-modeling can be applied in multiscale finite element simulations, as a surrogate model to replace the computationally expensive DEM RVEs. The example consists of a mixed-mode tension-shear test on a plane-strain granular specimen with embedded strong discontinuity. The sample is 0.1 m x 0.1 m in dimension. The bottom edge is fixed, while the top edge moves rigidly following a mixed-mode loading-unloading-reloading displacement path, as shown in Fig. 14. The sample is assumed periodic in the horizontal direction, thus periodic displacement boundary condition is applied on the lateral edges. The geometry of the pre-existing interface in the center is a sinusoid with the spatial period of 0.05 m and amplitude of 0.005 m. The elements along the interface are enhanced by assumed strain formulation to embed the strong discontinuity [Oliver et al., 2002], while the other elements are regular bulk finite elements. The optimal traction-separation model found in the Numerical Example 2 is applied in the interface. The bulk material is assumed isotropic linear elastic and the parameters are homogenized from the DEM RVE for generation of data (Young's modulus $E = 300$ MPa, Poisson's ratio $\nu = 0.24$). The specimen is initially under isotropic pressure of 10 MPa, the same as the DEM RVEs, and the lateral pressure remains constant during the loading steps.

The differential stress and strain fields computed by FEM-DRL multiscale approach at selected loading steps are shown in Fig. 15. The shear strain localizes in the embedded strong discontinuity in both specimens. The global traction-displacement curves in normal ($U_y - T_y$) and shear ($U_x - T_x$) directions are compared for both FEM-DRL and FEM-DEM simulations in Fig. 16. Results show great



(a) Violin plots of the density distribution of model scores in each DRL iteration (b) Mean value and \pm standard deviation of model score in each DRL iteration

Figure 11: Statistics of the model scores in deep reinforcement learning iterations from 5 separate runs of the DRL procedure for Numerical Experiment 2. Each DRL procedure contains ten iterations 0-9 of “exploration and exploitation” (by setting the temperature parameter $\tau = 1.0$) and a final iteration 10 of “competitive gameplay” ($\tau = 0.01$). Each iteration consists of 30 games. (a) Violin Plot of model scores played in each DRL iteration. The shade area represents the density distribution of scores. The white point represents the median. The thick black bar represents the interquartile range between 25% quantile and 75% quantile. The maximum and minimum scores played in each iteration are marked by horizontal lines. (b) Mean model score in each iteration and the error bars mark \pm standard deviation.

agreement on the mechanical behavior of the specimen. Hence the optimal traction-separation model automatically developed by the DRL meta-modeling approach can be used as a surrogate model to microscale DEM RVEs in multiscale FEM simulations.

7 Conclusion

This paper presents a meta-modeling approach in which we attempt to generate traction-separation laws not through explicitly writing a particular model but to provide the computer with modeling options such that it can explore on its own through self-practicing. Unlike previous deep-learning models that leverage supervised learning techniques to train neural networks that makes black-box predictions, this new approach focuses on reinforcement learning technique to discover hidden relationships among data and therefore make modeling decisions to emulate the process of writing constitutive models by human. Given the rules (frame indifference, thermodynamic laws, balance principles), we introduce an agenda-based approach where the DRL technique is used to find the optimal way to generate a forward prediction. As demonstrated in our numerical experiments, this approach can be regarded as a generalization of the previous models where neural network predictions may still embed in part of the predictions but are not necessarily completely replacing all components in the conventional models. This flexibility is the key for us to exploit the computer to make *repeated* trial-and-errors and improve from experiments over time to generate the best outcomes, instead of spending significant human time to explore through trial-and-errors. The idea of inventing the metal-

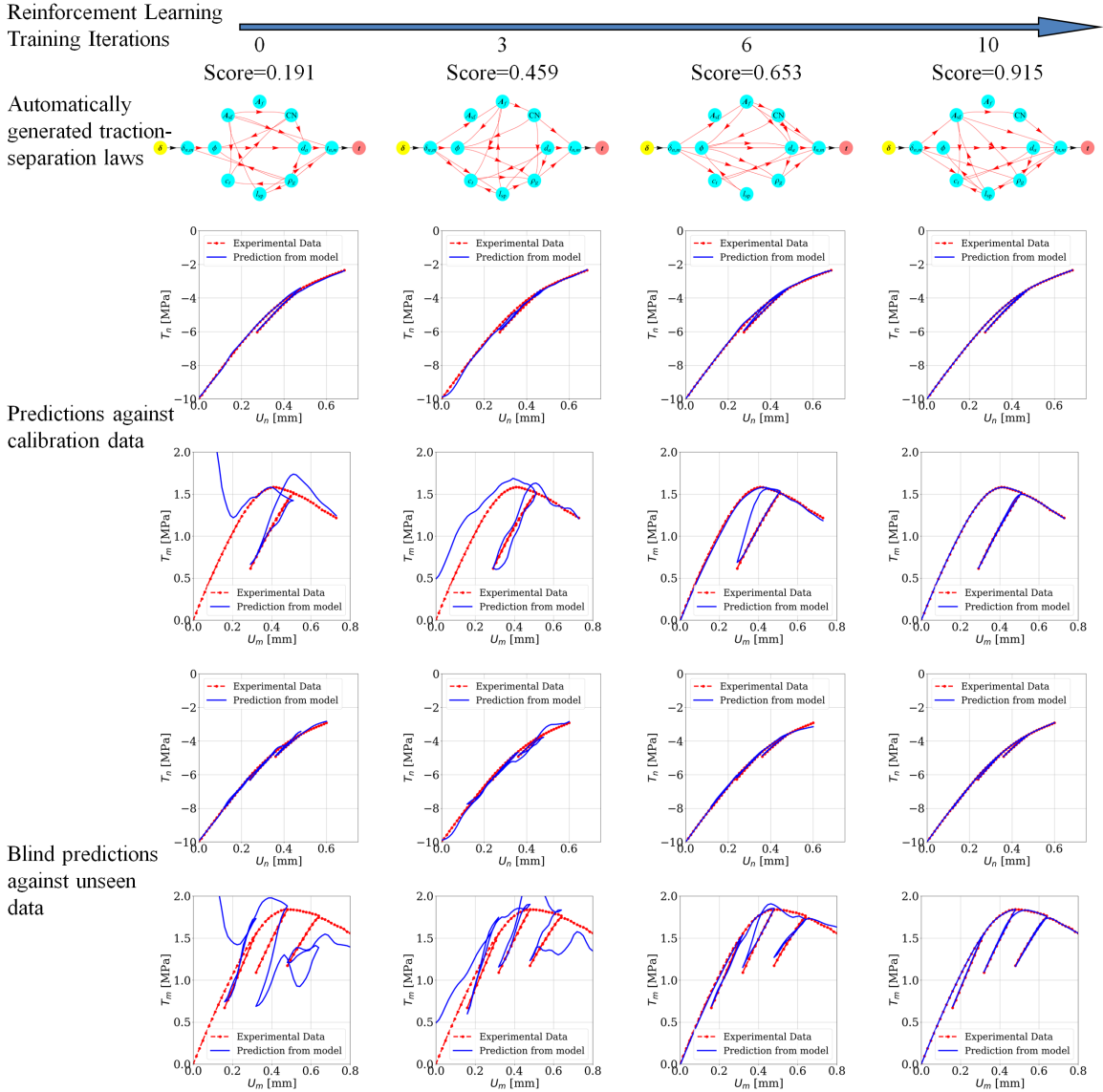


Figure 12: Knowledge of directed graphs of traction-separation models learned by deep reinforcement learning in Numerical Experiment 2.

modeling game could be significant in the sense that it frees modelers from focusing on curve-fitting a physical process. Instead, as future improvements on the models can be made by expanding the action space or simply leveraging the power of computer to improve the models over time, this allows us unprecedented luxury to place our focuses on finding best cause of actions that lead to the most predictive model. In addition, this meta-modeling approach also provides the following unique benefits against the conventional hand-crafting approach and black-box neural network models.

1. Since the machine learning procedure is automated, models intended for different purposes or designed to fulfill different demands (speed, accuracy, robustness) can be automatically generated and improved over time through self-plays in the model-creation game.
2. Since the validation procedure is introduced as the reward mechanism for the agent to find the

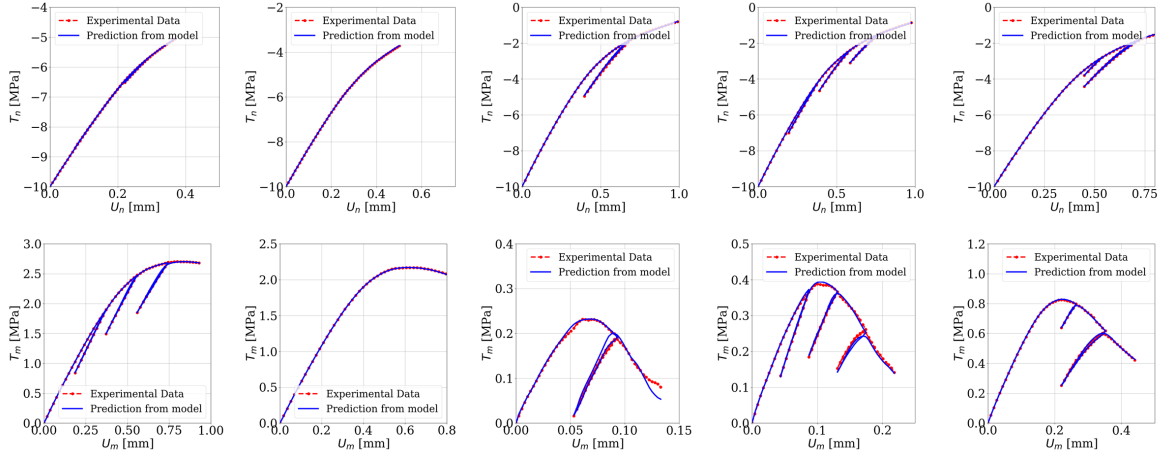


Figure 13: Five examples of blind predictions from the optimal digraph configuration (The 4th digraph in Figure 12) against unseen data among test database of 150 loading cases.

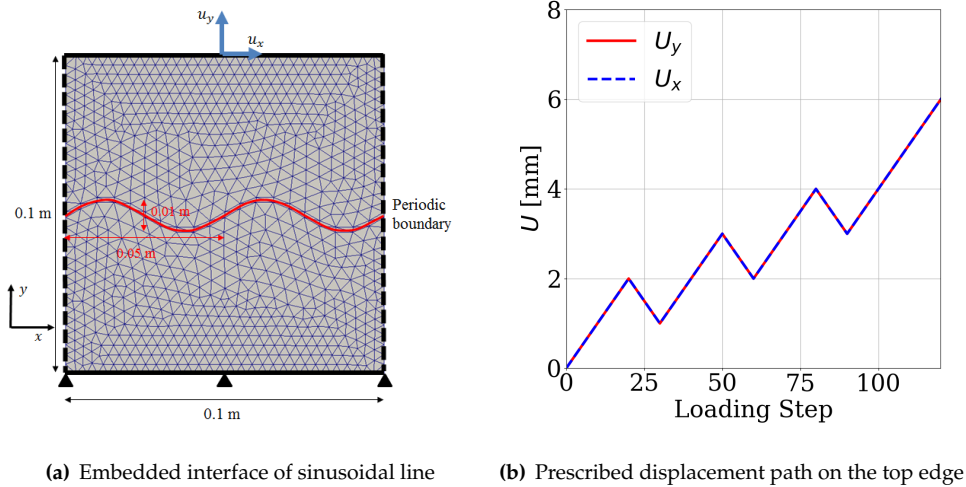


Figure 14: Plane-strain mixed-mode tension-shear test on a granular specimen with pre-existing interface. Geometry, mesh and boundary conditions.

optimal models available, the resultant models are always validated at the end of the games.

3. By recasting constitutive models as directed graphs, previous models established by domain experts can be easily embedded in the proposed framework to expand action spaces efficiently and shorten the training time.
4. The metal-modeling approach is generic and reusable, which means that it can handle different situations with different data, objective functions and rules set by human without going through additional derivation, implementation, material parameter identification and validation. Hence it does not require any debugging once the the game is implemented correctly.

There are also limitations of the current approaches. For instance, the demands for data could be higher than conventional modeling approach, particularly when more sophisticated and rigorous

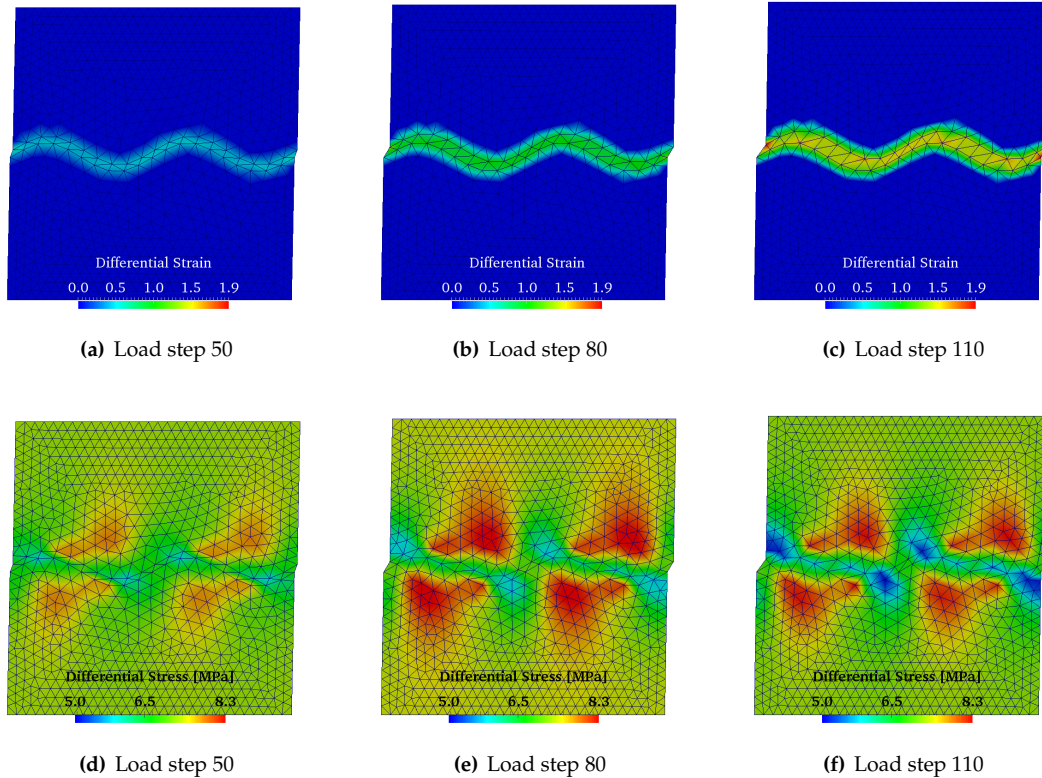
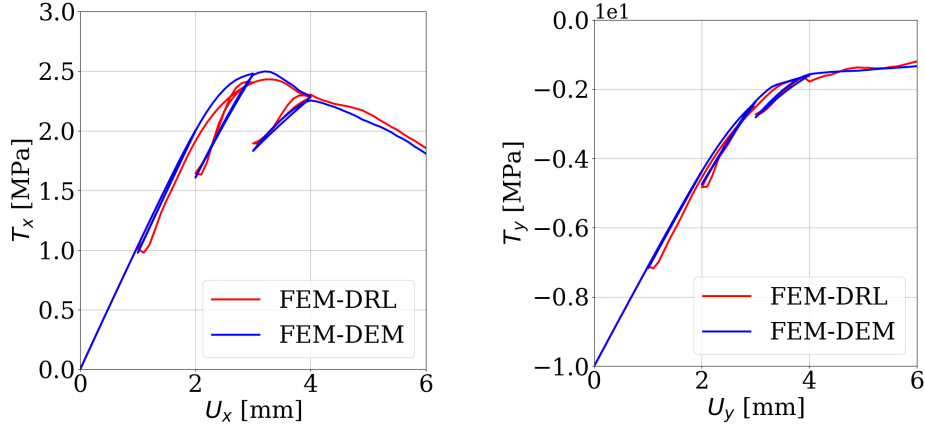


Figure 15: Differential stress field ($\sigma_1 - \sigma_3$, where σ_1 is the greatest principal value and σ_3 is the least principal value of the Cauchy stress tensor σ) and differential strain field ($\epsilon_1 - \epsilon_3$, where ϵ_1 is the greatest principal value and ϵ_3 is the least principal value of the strain tensor ϵ) at loading steps 50, 80 and 110 in the mixed-mode tension-shear test.

validation metric is used to assign model score and game reward. The model has not yet introduced any technique to handle noise, nor does it consider any mechanism to consider uncertainty. While these topics are of great importance, the corresponding research activities are beyond the scope of this study and will be considered in the future, should opportunities come.

Acknowledgments

The corresponding author's work is supported by the Earth Materials and Processes program from the US Army Research Office under grant contract W911NF-15-1-0442 and W911NF-15-1-0581, the Dynamic Materials and Interactions Program from the Air Force Office of Scientific Research under grant contract FA9550-17-1-0169, the nuclear energy university program from department of energy under grant contract DE-NE0008534 as well as the Mechanics of Material program at National Science Foundation under grant contract CMMI-1462760. Meanwhile, the first author is supported by US Army Research Office under grant contract W911NF-15-1-0442 and W911NF-15-1-0581, and the 2018 Interdisciplinary Research Seed funding from Columbia University. These supports are gratefully acknowledged. The views and conclusions contained in this document are those of the authors, and should not be interpreted as representing the official policies, either expressed or implied, of the sponsors, including the Army Research Laboratory or the U.S. Government. The U.S. Government is authorized to reproduce and distribute reprints for Government purposes notwithstanding any



(a) Embedded interface of sinusoidal line (b) Prescribed displacement path on the top edge

Figure 16: Comparison of FEM-DRL and FEM-DEM multiscale simulations on global traction-displacement relation in normal ($U_y - T_y$) and tangential ($U_x - T_x$) directions on the top edge of the specimen.

copyright notation herein.

Appendix A: Generation of synthetic data from discrete element modeling (DEM)

The data for calibration and evaluation of prediction accuracy of the deep-reinforcement-learned traction-separation models are generated by numerical simulations on a representative volume element (RVE) representing the granular materials on a frictional surface. The open-source software YADE for DEM is used [Šmilauer et al., 2010]. The discrete element particles in the RVE have radii between 1 ± 0.3 mm with uniform distribution. The RVE has the height of 20 mm in the normal direction of the frictional surface and is initially consolidated to isotropic pressure of 10 MPa. The Cundall’s elastic-frictional contact model ([Cundall and Strack, 1979]) is used for the inter-particle constitutive law. The material parameters are: interparticle elastic modulus $E_{eq} = 1$ GPa, ratio between shear and normal stiffness $k_s/k_n = 0.3$, frictional angle $\varphi = 30^\circ$, density $\rho = 2600$ kg/m³, Cundall damping coefficient $\alpha_{damp} = 0.2$.

The DEM RVE is loaded in the normal n and tangential m directions of the frictional surface by displacement controls δ_n and δ_m (Figure 17(a)). The synthetic database consists of 200 numerical experiments under different loading paths. They differ from each other in the ratio of normal and tangential loading rate $\dot{\delta}_n/\dot{\delta}_m$, as well as the loading-unloading-reloading cycles, as illustrated in Figure 17(b), 17(c) and 17(d). The traction-separation curves of the experiments are recorded and three examples corresponding to the paths in Figure 17 are presented in Figure 18. The microstructural information required for the intermediate nodes in the directed graphs, such as porosity, coordination number and fabric tensor, are also recorded during the simulations. The open-source library NetworkX [Hagberg et al., 2008] is employed to analyze the graph of the particle interactions in the RVEs. Figure 19 presents examples of microstructural information and graph characteristics for the three example loading paths. The 200 numerical simulations in the database are shuffled. The first 50 simulations are used as “training data” for the calibration of model parameters for the edges in the directed graphs. The other 150 simulations are “test data” only for evaluating the blind prediction accuracy of the

resultant constitutive model.

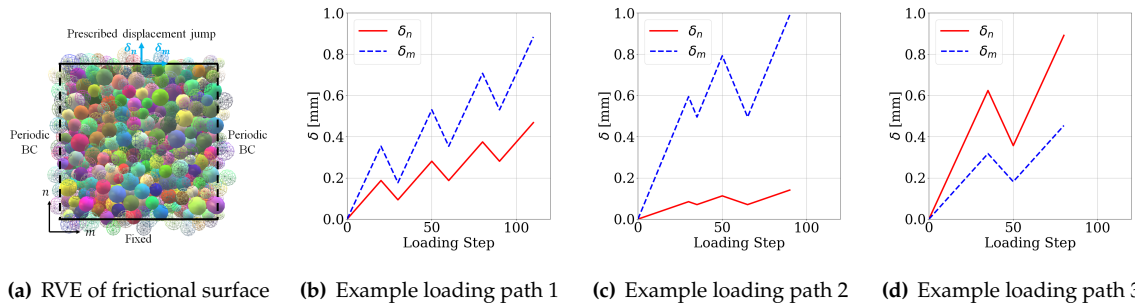


Figure 17: Representative volume element of a frictional surface having normal n and tangential m directions. Three examples of different loading-unloading-reloading paths among 200 numerical experiments for the generation of database are shown.

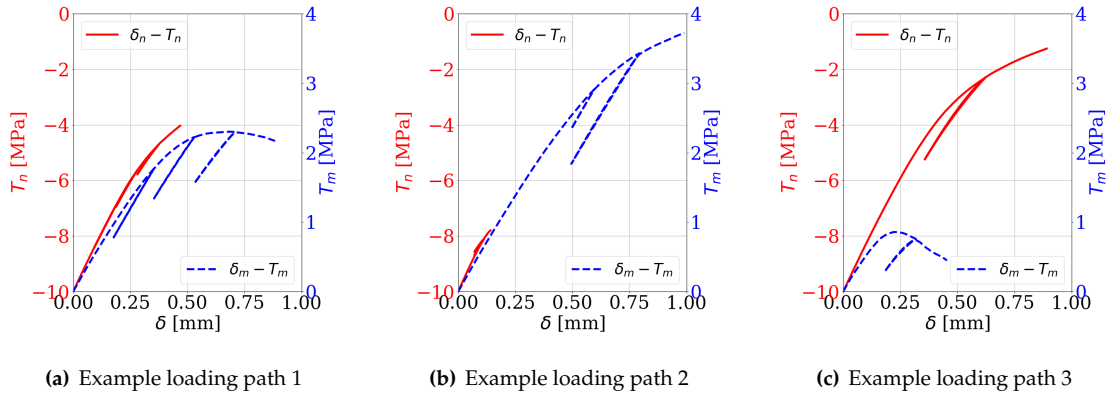


Figure 18: Examples of traction-separation curves corresponding to the three loading paths in Figure 17 among 200 numerical simulations. The normal traction T_n is plotted against the normal displacement jump δ_n . The tangential traction T_m is plotted against the tangential displacement jump δ_m .

References

- Theodore W Anderson and Donald A Darling. A test of goodness of fit. *Journal of the American statistical association*, 49(268):765–769, 1954.
- Jørgen Bang-Jensen and Gregory Z Gutin. *Digraphs: theory, algorithms and applications*. Springer Science & Business Media, 2008.
- Richard Bellman. A markovian decision process. *Journal of Mathematics and Mechanics*, pages 679–684, 1957.
- MA Bessa, R Bostanabad, Z Liu, A Hu, Daniel W Apley, C Brinson, W Chen, and Wing Kam Liu. A framework for data-driven analysis of materials under uncertainty: Countering the curse of dimensionality. *Computer Methods in Applied Mechanics and Engineering*, 320:633–667, 2017.

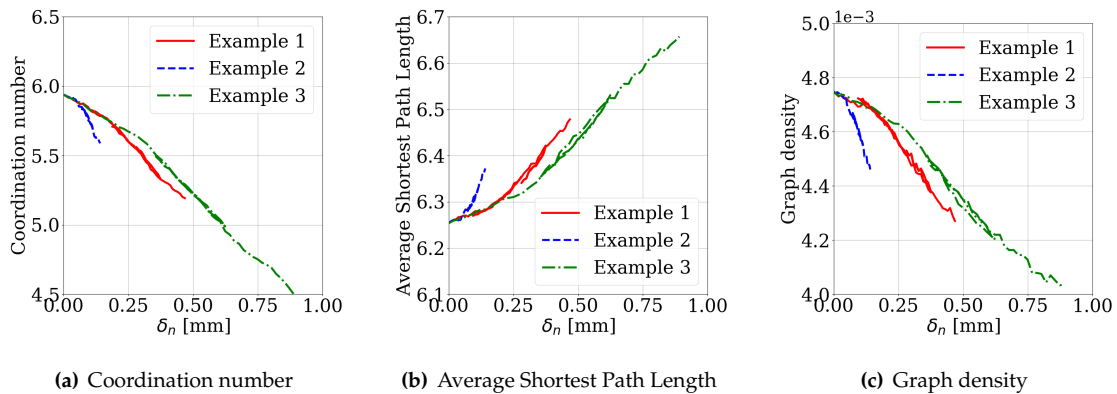


Figure 19: Examples of coordination number, average shortest path length and graph density for particle interactions corresponding to the three loading paths in Figure 17 among 200 numerical simulations. These quantities are plotted against the normal displacement jump δ_n .

Ronaldo I Borja. *Plasticity: modeling & computation*. Springer Science & Business Media, 2013.

Ronaldo I Borja and Craig D Foster. Continuum mathematical modeling of slip weakening in geological systems. *Journal of Geophysical Research: Solid Earth*, 112(B4), 2007.

Cameron B Browne, Edward Powley, Daniel Whitehouse, Simon M Lucas, Peter I Cowling, Philipp Rohlfshagen, Stephen Tavener, Diego Perez, Spyridon Samothrakis, and Simon Colton. A survey of monte carlo tree search methods. *IEEE Transactions on Computational Intelligence and AI in games*, 4(1):1–43, 2012.

Eric C. Bryant and WaiChing Sun. A mixed-mode phase field fracture model in anisotropic rocks with consistent kinematics. *Computer Methods in Applied Mechanics and Engineering*, 2018. ISSN 0045-7825. doi: <https://doi.org/10.1016/j.cma.2018.08.008>. URL <http://www.sciencedirect.com/science/article/pii/S0045782518303943>.

Kyunghyun Cho, Bart Van Merriënboer, Caglar Gulcehre, Dzmitry Bahdanau, Fethi Bougares, Holger Schwenk, and Yoshua Bengio. Learning phrase representations using rnn encoder-decoder for statistical machine translation. *arXiv preprint arXiv:1406.1078*, 2014.

François Chollet et al. Keras. <https://keras.io>, 2015.

Peter A Cundall and Otto DL Strack. A discrete numerical model for granular assemblies. *geotechnique*, 29(1):47–65, 1979.

Yannis F Dafalias and Majid T Manzari. Simple plasticity sand model accounting for fabric change effects. *Journal of Engineering mechanics*, 130(6):622–634, 2004.

Yannis F Dafalias, Achilleas G Papadimitriou, and Xiang S Li. Sand plasticity model accounting for inherent fabric anisotropy. *Journal of Engineering Mechanics*, 130(11):1319–1333, 2004.

I Capuzzo Dolcetta and Hitoshi Ishii. Approximate solutions of the bellman equation of deterministic control theory. *Applied Mathematics and Optimization*, 11(1):161–181, 1984.

MGGV Elices, GV Guinea, J Gomez, and J Planas. The cohesive zone model: advantages, limitations and challenges. *Engineering fracture mechanics*, 69(2):137–163, 2002.

- Tanvir R Faisal, Nicolay Hristozov, Tamara L Western, Alejandro D Rey, and Damiano Pasini. Computational study of the elastic properties of rheum rhabarbarum tissues via surrogate models of tissue geometry. *Journal of structural biology*, 185(3):285–294, 2014.
- Frédéric Feyel. A multilevel finite element method (fe2) to describe the response of highly non-linear structures using generalized continua. *Computer Methods in applied Mechanics and engineering*, 192(28-30):3233–3244, 2003.
- Jacob Fish. *Practical multiscale modeling*. John Wiley & Sons, 2013.
- Pengcheng Fu and Yannis F Dafalias. Fabric evolution within shear bands of granular materials and its relation to critical state theory. *International Journal for numerical and analytical methods in geomechanics*, 35(18):1918–1948, 2011.
- Aric Hagberg, Pieter Swart, and Daniel S Chult. Exploring network structure, dynamics, and function using networkx. Technical report, Los Alamos National Lab.(LANL), Los Alamos, NM (United States), 2008.
- CB Hirschberger, S Ricker, P Steinmann, and N Sukumar. Computational multiscale modelling of heterogeneous material layers. *Engineering Fracture Mechanics*, 76(6):793–812, 2009.
- Claudia Britta Hirschberger, Natarajan Sukumar, and Paul Steinmann. Computational homogenization of material layers with micromorphic mesostructure. *Philosophical Magazine*, 88(30-32):3603–3631, 2008.
- Sepp Hochreiter and Jürgen Schmidhuber. Long short-term memory. *Neural computation*, 9(8):1735–1780, 1997.
- Kurt Hornik, Maxwell Stinchcombe, and Halbert White. Multilayer feedforward networks are universal approximators. *Neural networks*, 2(5):359–366, 1989.
- Orion L Kafka, Cheng Yu, Modesar Shakoor, Zeliang Liu, Gregory J Wagner, and Wing Kam Liu. Data-driven mechanistic modeling of influence of microstructure on high-cycle fatigue life of nickel titanium. *JOM*, pages 1–5, 2018.
- Maurice George Kendall et al. The advanced theory of statistics. *The advanced theory of statistics.*, (2nd Ed), 1946.
- Shahriyar Keshavarz and Somnath Ghosh. Multi-scale crystal plasticity finite element model approach to modeling nickel-based superalloys. *Acta Materialia*, 61(17):6549–6561, 2013.
- Diederik P Kingma and Jimmy Ba. Adam: A method for stochastic optimization. *arXiv preprint arXiv:1412.6980*, 2014.
- Kedar Kirane and Somnath Ghosh. A cold dwell fatigue crack nucleation criterion for polycrystalline ti-6242 using grain-level crystal plasticity fe model. *International Journal of Fatigue*, 30(12):2127–2139, 2008.
- Matthew R Kuhn, WaiChing Sun, and Qi Wang. Stress-induced anisotropy in granular materials: fabric, stiffness, and permeability. *Acta Geotechnica*, 10(4):399–419, 2015.
- BA Le, Julien Yvonnet, and Q-C He. Computational homogenization of nonlinear elastic materials using neural networks. *International Journal for Numerical Methods in Engineering*, 104(12):1061–1084, 2015.
- M Lefik and BA Schrefler. Artificial neural network for parameter identifications for an elasto-plastic model of superconducting cable under cyclic loading. *Computers & structures*, 80(22):1699–1713, 2002.

- Xiang Song Li and Yannis F Dafalias. Anisotropic critical state theory: role of fabric. *Journal of Engineering Mechanics*, 138(3):263–275, 2011.
- Guang Liu, WaiChing Sun, Steven M Lowinger, ZhenHua Zhang, Ming Huang, and Jun Peng. Coupled flow network and discrete element modeling of injection-induced crack propagation and coalescence in brittle rock. *Acta Geotechnica*, pages 1–26, 2018.
- Yang Liu, WaiChing Sun, and Jacob Fish. Determining material parameters for critical state plasticity models based on multilevel extended digital database. *Journal of Applied Mechanics*, 83(1):011003, 2016a.
- Yang Liu, WaiChing Sun, Zifeng Yuan, and Jacob Fish. A nonlocal multiscale discrete-continuum model for predicting mechanical behavior of granular materials. *International Journal for Numerical Methods in Engineering*, 106(2):129–160, 2016b.
- Morteza M Mehrabadi, S Nemat-Nasser, and M Oda. On statistical description of stress and fabric in granular materials. *International Journal for Numerical and Analytical Methods in Geomechanics*, 6(1): 95–108, 1982.
- Nicolas Moës, Mathieu Cloirec, Patrice Cartraud, and J-F Remacle. A computational approach to handle complex microstructure geometries. *Computer methods in applied mechanics and engineering*, 192(28-30):3163–3177, 2003.
- SeonHong Na and WaiChing Sun. Computational thermo-hydro-mechanics for multiphase freezing and thawing porous media in the finite deformation range. *Computer Methods in Applied Mechanics and Engineering*, 318:667–700, 2017.
- Nasser M Nasrabadi. Pattern recognition and machine learning. *Journal of electronic imaging*, 16(4): 049901, 2007.
- Mitiyasu Ohnaka and Teruo Yamashita. A cohesive zone model for dynamic shear faulting based on experimentally inferred constitutive relation and strong motion source parameters. *Journal of Geophysical Research: Solid Earth*, 94(B4):4089–4104, 1989.
- J Oliver, Alfredo Edmundo Huespe, MDG Pulido, and E Chaves. From continuum mechanics to fracture mechanics: the strong discontinuity approach. *Engineering fracture mechanics*, 69(2):113–136, 2002.
- Michael Ortiz and Anna Pandolfi. Finite-deformation irreversible cohesive elements for three-dimensional crack-propagation analysis. *International journal for numerical methods in engineering*, 44(9):1267–1282, 1999.
- Sinno Jialin Pan, Qiang Yang, et al. A survey on transfer learning. *IEEE Transactions on knowledge and data engineering*, 22(10):1345–1359, 2010.
- Jitesh H Panchal, Surya R Kalidindi, and David L McDowell. Key computational modeling issues in integrated computational materials engineering. *Computer-Aided Design*, 45(1):4–25, 2013.
- Kyoungsoo Park, Glaucio H Paulino, and Jeffery R Roesler. A unified potential-based cohesive model of mixed-mode fracture. *Journal of the Mechanics and Physics of Solids*, 57(6):891–908, 2009.
- M Pastor, AHC Chan, P Mira, D Manzanal, JA Fernández Merodo, and T Blanc. Computational geomechanics: the heritage of olek zienkiewicz. *International Journal for Numerical Methods in Engineering*, 87(1-5):457–489, 2011.
- Mervyn S Paterson and Teng-fong Wong. *Experimental rock deformation-the brittle field*. Springer Science & Business Media, 2005.

- F. Pedregosa, G. Varoquaux, A. Gramfort, V. Michel, B. Thirion, O. Grisel, M. Blondel, P. Prettenhofer, R. Weiss, V. Dubourg, J. Vanderplas, A. Passos, D. Cournapeau, M. Brucher, M. Perrot, and E. Duchesnay. Scikit-learn: Machine learning in Python. *Journal of Machine Learning Research*, 12:2825–2830, 2011.
- Timon Rabczuk and PMA Areias. A new approach for modelling slip lines in geological materials with cohesive models. *International Journal for Numerical and Analytical Methods in Geomechanics*, 30(11):1159–1172, 2006.
- James R Rice. A path independent integral and the approximate analysis of strain concentration by notches and cracks. *Journal of applied mechanics*, 35(2):379–386, 1968.
- John W Rudnicki. Fracture mechanics applied to the earth’s crust. *Annual Review of Earth and Planetary Sciences*, 8(1):489–525, 1980.
- Andrew G Salinger, Roscoe A Bartlett, Andrew M Bradley, Qiushi Chen, Irina P Demeshko, Xujiao Gao, Glen A Hansen, Alejandro Mota, Richard P Muller, Erik Nielsen, et al. Albany: using component-based design to develop a flexible, generic multiphysics analysis code. *International Journal for Multiscale Computational Engineering*, 14(4), 2016.
- Fritz W Scholz and Michael A Stephens. K-sample anderson–darling tests. *Journal of the American Statistical Association*, 82(399):918–924, 1987.
- Claude E Shannon. Xxii. programming a computer for playing chess. *The London, Edinburgh, and Dublin Philosophical Magazine and Journal of Science*, 41(314):256–275, 1950.
- David Silver, Aja Huang, Chris J Maddison, Arthur Guez, Laurent Sifre, George Van Den Driessche, Julian Schrittwieser, Ioannis Antonoglou, Veda Panneershelvam, Marc Lanctot, et al. Mastering the game of go with deep neural networks and tree search. *nature*, 529(7587):484–489, 2016.
- David Silver, Thomas Hubert, Julian Schrittwieser, Ioannis Antonoglou, Matthew Lai, Arthur Guez, Marc Lanctot, Laurent Sifre, Dhharshan Kumaran, Thore Graepel, et al. Mastering chess and shogi by self-play with a general reinforcement learning algorithm. *arXiv preprint arXiv:1712.01815*, 2017a.
- David Silver, Julian Schrittwieser, Karen Simonyan, Ioannis Antonoglou, Aja Huang, Arthur Guez, Thomas Hubert, Lucas Baker, Matthew Lai, Adrian Bolton, et al. Mastering the game of go without human knowledge. *Nature*, 550(7676):354, 2017b.
- Václav Šmilauer, Emanuele Catalano, Bruno Chareyre, Sergei Dorofeenko, Jerome Duriez, Anton Gladky, Janek Kozicki, Chiara Modenese, Luc Scholtès, Luc Sibille, et al. Yade reference documentation. *Yade Documentation*, 474(1), 2010.
- Wai Ching Sun, Jose E Andrade, and John W Rudnicki. Multiscale method for characterization of porous microstructures and their impact on macroscopic effective permeability. *International Journal for Numerical Methods in Engineering*, 88(12):1260–1279, 2011a.
- WaiChing Sun. A unified method to predict diffuse and localized instabilities in sands. *Geomechanics and Geoengineering*, 8(2):65–75, 2013.
- WaiChing Sun. A stabilized finite element formulation for monolithic thermo-hydro-mechanical simulations at finite strain. *International Journal for Numerical Methods in Engineering*, 103(11):798–839, 2015.
- WaiChing Sun and Teng-fong Wong. Prediction of permeability and formation factor of sandstone with hybrid lattice boltzmann/finite element simulation on microtomographic images. *International Journal of Rock Mechanics and Mining Sciences*, 106:269–277, 2018.

- WaiChing Sun, José E Andrade, John W Rudnicki, and Peter Eichhubl. Connecting microstructural attributes and permeability from 3d tomographic images of in situ shear-enhanced compaction bands using multiscale computations. *Geophysical Research Letters*, 38(10), 2011b.
- WaiChing Sun, Matthew R Kuhn, and John W Rudnicki. A multiscale dem-lbm analysis on permeability evolutions inside a dilatant shear band. *Acta Geotechnica*, 8(5):465–480, 2013a.
- WaiChing Sun, Jakob T Ostien, and Andrew G Salinger. A stabilized assumed deformation gradient finite element formulation for strongly coupled poromechanical simulations at finite strain. *International Journal for Numerical and Analytical Methods in Geomechanics*, 37(16):2755–2788, 2013b.
- WaiChing Sun, Qiushi Chen, and Jakob T Ostien. Modeling the hydro-mechanical responses of strip and circular punch loadings on water-saturated collapsible geomaterials. *Acta Geotechnica*, 9(5):903–934, 2014.
- Richard S Sutton. Introduction: The challenge of reinforcement learning. In *Reinforcement Learning*, pages 1–3. Springer, 1992.
- Aaron E Tallman, Laura P Swiler, Yan Wang, and David L McDowell. Reconciled top-down and bottom-up hierarchical multiscale calibration of bcc fe crystal plasticity. *International Journal for Multiscale Computational Engineering*, 15(6), 2017.
- Stephen Timoshenko. *History of strength of materials: with a brief account of the history of theory of elasticity and theory of structures*. Courier Corporation, 1953.
- Antoinette Tordesillas, David M Walker, and Qun Lin. Force cycles and force chains. *Physical Review E*, 81(1):011302, 2010.
- Antoinette Tordesillas, David M Walker, Amy L Rechenmacher, and Sara Abedi. Discovering community structures and dynamical networks from grain-scale kinematics of shear bands in sand. In *Advances in Bifurcation and Degradation in Geomaterials*, pages 67–73. Springer, 2011.
- Clemens V Verhoosel, Joris JC Remmers, Miguel A Gutiérrez, and Rene De Borst. Computational homogenization for adhesive and cohesive failure in quasi-brittle solids. *International Journal for Numerical Methods in Engineering*, 83(8-9):1155–1179, 2010.
- Daniele Versino, Alberto Tonda, and Curt A Bronkhorst. Data driven modeling of plastic deformation. *Computer Methods in Applied Mechanics and Engineering*, 318:981–1004, 2017.
- Kun Wang and WaiChing Sun. Anisotropy of a tensorial bishop’s coefficient for wetted granular materials. *Journal of Engineering Mechanics*, 143(3):B4015004, 2015.
- Kun Wang and WaiChing Sun. A semi-implicit discrete-continuum coupling method for porous media based on the effective stress principle at finite strain. *Computer Methods in Applied Mechanics and Engineering*, 304:546–583, 2016.
- Kun Wang and WaiChing Sun. A unified variational eigen-erosion framework for interacting brittle fractures and compaction bands in fluid-infiltrating porous media. *Computer Methods in Applied Mechanics and Engineering*, 318:1–32, 2017.
- Kun Wang and WaiChing Sun. A multiscale multi-permeability poroplasticity model linked by recursive homogenizations and deep learning. *Computer Methods in Applied Mechanics and Engineering*, 334:337–380, 2018.
- Kun Wang, Waiching Sun, Simon Salager, S Na, and Ghonwa Khaddour. Identifying material parameters for a micro-polar plasticity model via x-ray micro-ct images: lessons learned from the curve-fitting exercises. *International Journal for Multiscale Computational Engineering*, 14(4):389–413, 2016.

John R Williams and Nabha Rege. Coherent vortex structures in deforming granular materials. *Mechanics of Cohesive-frictional Materials: An International Journal on Experiments, Modelling and Computation of Materials and Structures*, 2(3):223–236, 1997.

Huanran Wu, Ning Guo, and Jidong Zhao. Multiscale modeling and analysis of compaction bands in high-porosity sandstones. *Acta Geotechnica*, 13(3):575–599, 2018.

Stephan Wulfinghoff, Fabiola Cavaliere, and Stefanie Reese. Model order reduction of nonlinear homogenization problems using a hashin–shtrikman type finite element method. *Computer Methods in Applied Mechanics and Engineering*, 330:149–179, 2018.